Quantification of the influencing factors for flood peak discharge increase in the Lower Yellow River

Li, Wei; Zhu, Lehong; Xie, Guohu; Hu, Peng; de Vriend, Huib J.

DOI
10.1016/j.jhydrol.2022.128329

Publication date
2022

Document Version
Final published version

Published in
Journal of Hydrology

Citation (APA)
Li, W., Zhu, L., Xie, G., Hu, P., & de Vriend, H. J. (2022). Quantification of the influencing factors for flood peak discharge increase in the Lower Yellow River. *Journal of Hydrology*, *613*, Article 128329. https://doi.org/10.1016/j.jhydrol.2022.128329

Journal of Hydrology 613 (2022) 128329

Contents lists available at ScienceDirect

Journal of Hydrology

journal homepage: www.elsevier.com/locate/jhydrol

Research papers

Quantification of the influencing factors for flood peak discharge increase in the Lower Yellow River

Wei Li [a,*], Lehong Zhu [a], Guohu Xie [a], Peng Hu [a,b], Huib J. de Vriend [c]

[a] Ocean College, Zhejiang University, Hangzhou/Zhoushan, 310058, China
[b] Ocean Research Center of Zhoushan, Zhejiang University, Zhoushan 316021, China
[c] Faculty of Civil Engineering and Geosciences, Delft University of Technology, P. O. Box 5048, 2600 GA Delft, the Netherlands

ARTICLE INFO

This manuscript was handled by Marco Borga, Editor-in-Chief, with the assistance of Hanbo Yang, Associate Editor

Keywords:
River flood
Hyperconcentrated flow
Peak discharge increase
Lower Yellow River
Influencing factor

ABSTRACT

The past decades have witnessed frequent flood peak discharges increase in the Lower Yellow River (LYR). Yet no consensus for its mechanism has been achieved. Here 21 events of the peak discharge increase (PDI) in the period of 1973–2012 are analysed. It is shown that the mean increment of peak discharge increases from 810 m^3/s to 1158 m^3/s and the frequency also increases from once every 2 years to once every 1.5 years after the completion of Xiaolangdi (XLD) Reservoir. Afterwards, the ordinary differential equations (ODEs) along the characteristics for the discharge are derived, from which seven factors (terms I ~ VII) that may affect the discharge variation are identified: the effects related to the longitudinal change in flow density (I), and in the product of flow density and flow area (II); the pressure terms due to river width gradient (III) and flow density (IV); the external forces (V); the momentum term due to bed deformation (VI); and the imbalanced advection (VII). Using field data of the 21 events, the bed Manning roughness is back-calculated from the ordinary discharge equation, which agrees with the documented values very well. Quantitative comparisons of the seven factors indicate that the pressure term due to the river width gradient plays a major role in promoting the PDI in most events, whereas the external forces term is the primary cause that attenuates PDI. The rest influencing factors have marginal effects with a much smaller magnitude.

1. Introduction

The Yellow River is noted for the huge amount of sediment it carries from the Loess Plateau (Wang et al., 2022; Xu et al., 2022). A consequence of the heavy sediment load is widespread flooding in vulnerable regions, causing serious casualties in history (Singh et al., 2021; Tian et al., 2019). Consequently, the Yellow River flooding has been a major disaster to Chinese people. In ancient times, the mainstream of the Lower Yellow River (LYR) shifted frequently due to the easily erodible river bed and banks, as well as the very high sediment overloading. At the time of the Ming Dynasty, this problem was partly alleviated by the strategy of "building high levees, and thus clearing sediments by converging flow" (Wang and Liu, 2019). Nevertheless, this has caused a "perched river" in the lower reach, where an abnormal phenomenon of downstream flooding peak discharge increase (PDI) has been noted, mostly in the reach from Xiaolangdi (XLD) to Huanyuankou (HYK) and farther to Jiahetan (JHT) (Fig. 1**a**). An illustrative example is shown in Fig. 1**b**: the flood peak discharge at HYK station is much higher than that at the XLD station. Since the PDI phenomenon may greatly aggravate flood risks, much attention has been paid to its forming mechanism (Li, 2008; Li et al., 2014, 2017; Qi et al., 2011).

There have been two types of PDIs depending on whether the floodplain is inundated. For PDIs before the completion of the XLD Reservoir in 1999, floods often inundate the floodplain, and it has been proposed that both strong erosion and the interaction between the main channel and the floodplain may play important roles for these PDIs. For example, Wang et al. (2009) inferred that the main channel erosion and floodplain deposition may transit a wide-shallow channel to a narrow-deep channel, leading to acceleration of the flood propagation and subsequently overlap of flood waves. Qi and Li (1996) suggested that the main channel erosion and floodplain deposition may increase the water surface gradient between the main channel and the floodplain, accelerating the water flowing from the floodplain to the channel. This could add to a next flood, thus resulting in a PDI. Li et al. (2017) simulated the hyperconcentrated flood (HF) of August 1992 in a schematized representation of the channel-floodplain system in the LYR. This study

* Corresponding author at: Zhoushan Campus, Zhejiang University, No. 1 zheda Road, Dinghai District, Zhoushan City, Zhejiang Province, China.
E-mail address: lw05@zju.edu.cn (W. Li).

https://doi.org/10.1016/j.jhydrol.2022.128329
Received 17 May 2022; Received in revised form 5 August 2022; Accepted 7 August 2022
Available online 23 August 2022

successfully reproduced the morphological features of channel erosion and floodplain deposition, which is an important basis for those previous explanations (Qi and Li, 1996; Wang et al., 2009). Moreover, some scholars have highlighted the role of strong bed erosion during the flooding process (Cao et al., 2012, 2006; Dong et al., 2012; Kuang et al., 1999; Li et al., 2014; Wan and Wang, 1994). Cao et al. (2006, 2012) numerically investigated the 1977 HF (in the Xiaobeiganliu reach of the Middle Yellow River) and the 1992 HF (in the Lower Yellow River) in a schematic channel. These indicate that sufficient bed erosion can lead to considerable increase in the volume of water–sediment mixture and thus a PDI event. Similar findings were reported by Qi et al. (2011) and Li et al. (2014) when analysing the field data of the 1977 HF. Based on the eigenvalues of the governing equations, Ding et al. (2010) also suggested that considerable bed deformations may play a significant role in the propagation of shallow water waves.

After the XLD Reservoir became operational in October 1999, floods are mainly constrained within the relatively deep channel without floodplain inundation. For such in-channel flooding PDIs, the following mechanisms have been proposed. First, the tail of the flood can be accelerated by hyperconcentration-induced drag reduction and catch up with the peak, thus yielding a PDI (Jiang et al., 2006; Li et al., 2014). The opinion of drag reduction is mainly motivated by experimental data between the drag coefficient and the sediment concentration (Einstein and Chien, 1955; Vanoni, 1946; Wang et al., 1998; Zhu and Hao, 2008). Relevant arguments include the hyperconcentration-related turbulence damping (Van Maren et al., 2009b; Winterwerp, 2001, 2006; Winterwerp et al., 2009; Zhang, 1963) the increase of viscous sublayer thickness in hyperconcentrated circumstances (Gust, 1976), and a reduced of form drag by lack of sand dunes (Qi and Sun, 2013; Wan, 1985). In contrast, Ma et al. (2017) reported that flood conditions in the Lower Yellow River approach the upper plane bed regime, so large-scale sand dunes may not exist. Second, the PDI is possibly caused by the instability during flood propagation (Zhong et al., 2013). Near-bed flow may behave as a Bingham fluid and form a stagnant layer (Engelund and Wan, 1984; Wan and Wang, 1994; Wang, 2002; Wang and Chien, 1984) below the main flow region dominated by turbulent Newtonian flow. If the propagating dynamic wave behaves as a reverse diffusion process, the stagnant layer may become unstable and mix with the flow above, thus contributing to the PDI. On the other hand, Qi and Sun (2013) argue that flood flow in the Lower Yellow River is fully turbulent (Chien, 1989; Chien and Wan, 1999; Van Maren et al., 2009a; Wang, 2002), and that river clogging and instability of laminar flows will rarely happen.

Physically, flood wave propagation can be described by the shallow water equations (SWEs). Since the SWEs are hyperbolic, they can be rewritten as a set of ordinary compatibility equations along the characteristics. Therefore, ordinary differential equations (ODEs) for the discharge are derived here, which facilitate an analytical investigation of the main contributors for discharge variations. From the ordinary discharge equations, influencing factors that may affect the discharge variation are identified and quantified using field data of 21 PDI events in the LYR. The validity of these understandings is supported by the satisfactory agreements between the back-calculated Manning roughness and the documented roughness values. Section 2 reviews the 21 PDI flood events during 1973–2012 as the data preparation, and the detailed derivation and application of the ODEs are also introduced in Section 2. In Section 3, the model validation and the contributions of influencing terms are analysed. Uncertainties for these analyses are discussed in Section 4. Finally, we summarize conclusions in Section 5.

2. Materials and methods

2.1. Data preparation

The PDI phenomenon usually occurs at the XLD−HYK−JHT reach in the LYR (Fig. 1). The Yellow River Conservancy Commission (YRCC) has documented hydrological data of these three stations. From these data, 12 PDI events are identified during 1973–1999 (before the completion of the XLD Reservoir), and 9 PDI events are identified during 1999–2012. This means approximately one PDI event occurs every two years before 1999, but every one and a half years after 1999. Table 1 summarized some specific hydrographic and morphological data of the 12 + 9 PDI events at the three stations. For the XLD and HYK stations, the following data are given: the time for occurrence of the peak discharge (Date and clock); the flood peak discharge (Q), the flow area (A), and the river width at the water surface (B), the volumetric sediment concentration (c) corresponding to the peak discharge; the change

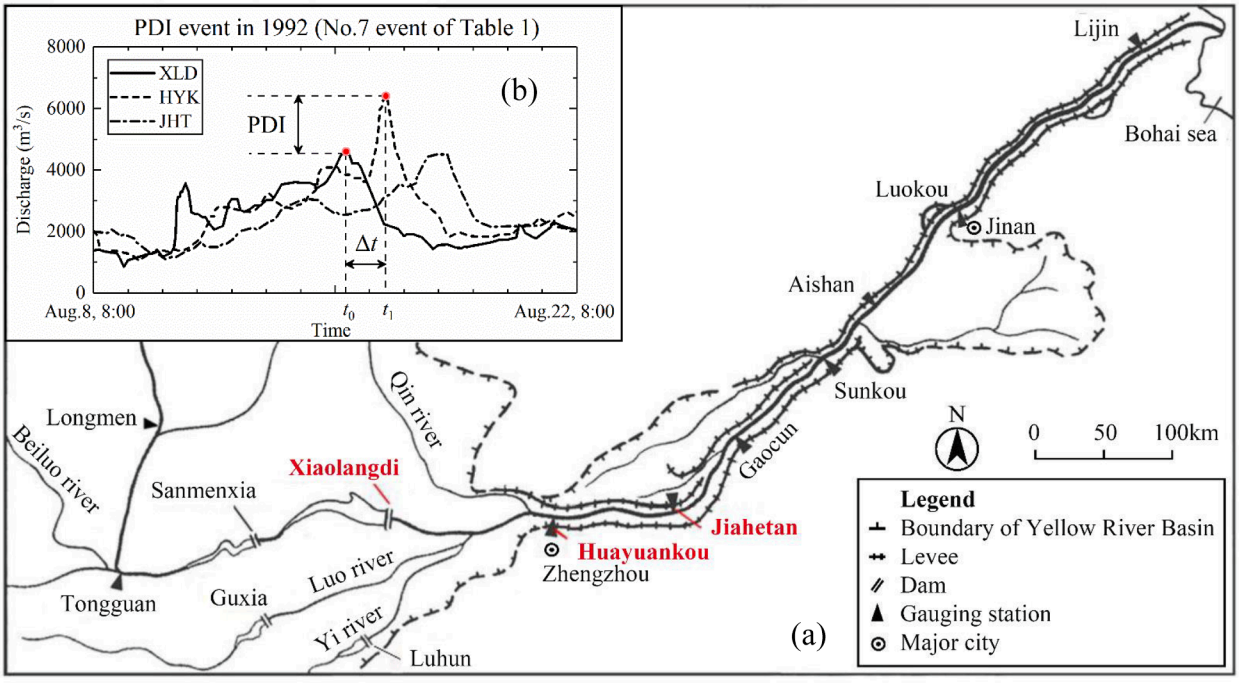

Fig. 1. (a) Sketch of the Lower Yellow River (adapted from Wu et al., 2008), (b) illustration of a PDI event using the 1992 flood as an example.

Table 1
Basic hydrographic and morphological data of the 21 floods.

Stage	No.	Peak time at XLD		Xiaolangdi					Peak time at HYK		Huayuankou					Jiahetan					Propagation time
		Date	Clock	Q(m^3/s)	A (m^2)	B(m)	c(m^3/m^3)	ΔA_s(m^2)	Date	Clock	Q(m^3/s)	A (m^2)	B(m)	c(m^3/m^3)	ΔA_s(m^2)	Q (m^3/s)	A (m^2)	B(m)	c(m^3/m^3)	ΔA_s(m^2)	Δt_i(h)
1973	1	1973.08.27	01:42	4320	1250	240	0.042	−780	1973.08.28	11:00	4710	2890	3190	0.045	1210	1550	792	524	0.034	639	33.3
-	2	1973.09.02	12:00	4400	1640	214	0.125	−780	1973.09.03	10:00	5890	2420	1620	0.128	1210	4440	1710	934	0.058	639	22
1999	3	1977.08.04	15:00	6960	2100	256	0.051	−216	1977.08.04	23:00	7320	2950	1150	0.033	2447	1710	2240	523	0.017	7274	8
	4	1977.08.07	21:00	10,100	2510	259	0.318	−216	1977.08.08	12:48	10,800	3840	2540	0.165	2447	3020	1540	485	0.057	7274	15.8
	5	1992.08.12	08:00	3050	1130	349	0.078	−94	1992.08.13	09:00	3230	1460	1430	0.048	7297	1700	785	684	0.037	389	25
	6	1992.08.14	04:00	3600	1260	357	0.159	−94	1992.08.15	00:00	4080	1650	617	0.087	7297	2930	1520	1400	0.035	389	20
	7	1992.08.15	15:42	4550	1600	380	0.198	−94	1992.08.16	19:00	6430	3570	1630	0.086	7297	2530	973	567	0.057	389	27.3
	8	1992.08.23	16:00	3180	1140	357	0.022	−94	1992.08.23	22:00	3340	1420	533	0.018	7297	2400	803	312	0.015	389	6
	9	1992.09.02	16:54	3400	1320	359	0.038	−94	1992.09.03	07:00	3660	1440	561	0.035	7297	2860	1340	1130	0.035	389	14.1
	10	1996.07.18	04:00	2880	1150	364	0.154	1695	1996.07.18	13:36	3400	1440	1000	0.026	257	842	550	440	0.011	885	9.6
	11	1996.08.04	00:00	5020	1570	364	0.088	1695	1996.08.05	15:30	7860	4470	3160	0.024	257	2960	1830	1530	0.029	885	39.5
	12	1996.08.12	04:00	5090	1670	364	0.053	1695	1996.08.13	03:30	5560	1560	599	0.046	257	3670	1580	594	0.016	885	23.5
	Average			4713	1528	322	0.111				5523	2426	1503	0.062		2551	1305	760	0.033		
1999	13	2004.08.23	02:54	2590	1260	320	0.056	281	2004.08.24	01:00	4150	1930	575	0.014	−253	875	662	516	0.001	−245	22.1
-	14	2004.08.26	10:00	2430	1150	323	0.050	281	2004.08.27	00:00	2730	1590	445	0.024	−253	1060	866	690	0.067	−245	14
2012	15	2005.07.06	12:00	2380	1190	1003	0.047	31	2005.07.07	05:24	3640	1520	1123	0.010	−6032	680	958	978	0.001	−6786	17.4
	16	2006.08.03	16:42	2080	1080	323	0.003	−71	2006.08.04	08:30	3360	2150	705	0.003	384	1340	972	504	0.001	1432	15.8
	17	2008.06.30	10:18	4050	1680	382	0.041	−116	2008.07.01	10:36	4600	2580	765	0.009	704	3870	1530	580	0.001	170	24.3
	18	2010.07.04	17:00	3580	1500	332	0.073	−77	2010.07.05	12:36	6600	5690	1200	0.018	−369	2600	1370	447	0.001	−1065	19.6
	19	2010.07.27	22:00	2290	1090	324	0.012	−77	2010.07.30	04:00	3100	1270	364	0.008	−369	2600	1240	400	0.003	−1065	54
	20	2011.07.04	21:18	2680	1250	330	0.100	10	2011.07.05	20:00	3900	1670	489	0.003	−405	2890	1480	421	0.002	−228	22.7
	21	2012.07.05	14:00	3050	1330	326	0.020	−99	2012.07.06	00:00	3470	2120	788	0.017	−49	1600	1370	448	0.002	370	10
	Average			2792	1281	407	0.045				3950	2280	717	0.012		1946	1161	554	0.009		

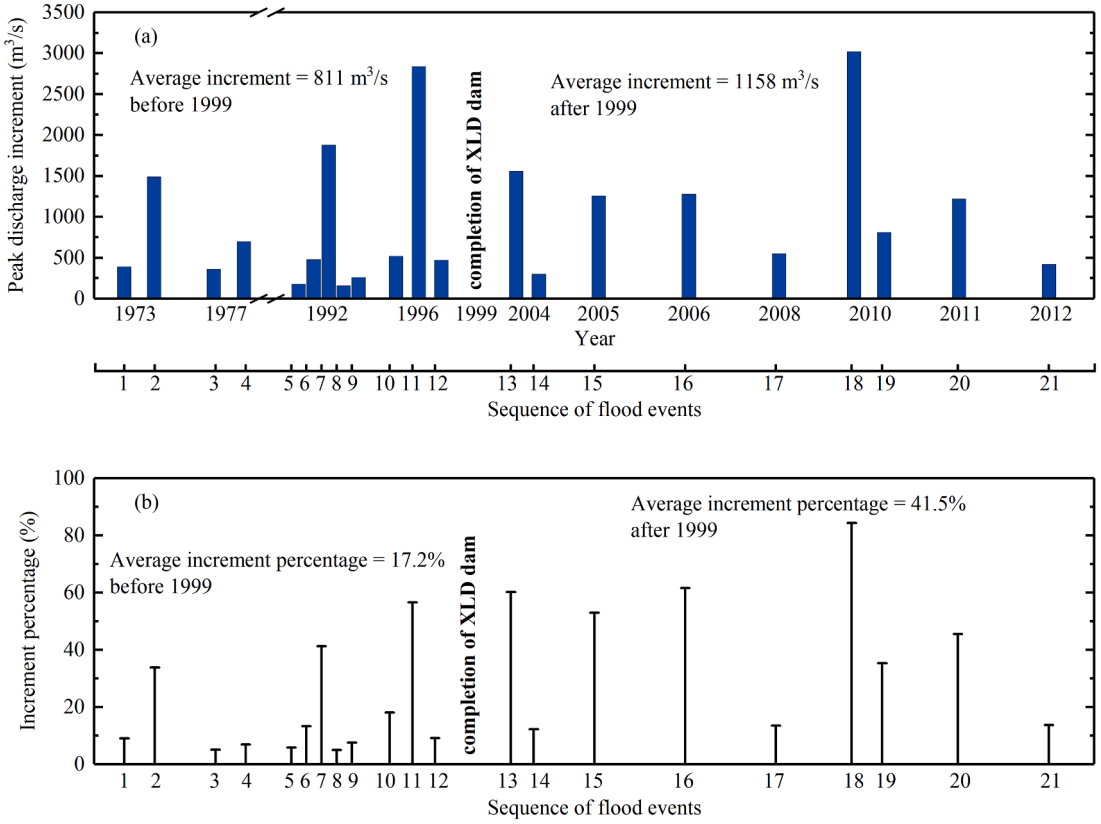

Fig. 2. (a) Peak discharge increment and (b) increment percentage between XLD and HYK station.

of the bed area at cross section over the flooding event (ΔA_s). For the JHT station, the timings for these measured data are not the time when the peak discharge arrives at JHT. Instead, the time for the measured data of JHT corresponds to the time of the peak discharge at XLD. The propagation time of peak discharge from XLD to HYK (Δt_i) is also shown in Table 1 (see the last column, which is calculated by 10 ~ 11 column minus 3 ~ 4 column). Fig. 2 presents the statistics of these 21 PDI events, including the discharge increase magnitude (Q_{HYK}-Q_{XLD}) from XLD to HYK (Fig. 2**a**) and the increasing percentage (Q_{HYK}-Q_{XLD})/Q_{XLD} (Fig. 2**b**).

From Table 1 and Fig. 2, the averaged peak discharge increment and increasing percentage are 810 m^3/s and 17.2 % before 1999. In contrast, these are 1158 m^3/s and 41.5 % after 1999, which are much larger than those before 1999. Nevertheless, the averaged peak discharges before 1999 are 4713 m^3/s at XLD and 5523 m^3/s at HYK, which is much larger than those after 1999: 2792 m^3/s at XLD, and 3950 m^3/s at HYK. These indicate that, although the flow discharge has been modulated greatly due to the XLD Reservoir, the PDI phenomenon has become more and more serious (higher frequency, larger increasing increment and higher increasing percentage of discharges).

2.2. Derivation and application of ODEs

This section introduces the ODEs derived along the characteristics and discuss their application and applicability. Specifically, the ODEs are derived in Section 2.2.1. In Section 2.2.2, we propose two strategies applied to obtain the formulations for discharge variation. And the applicability of the deduced ODEs for the LYR is explored in Section 2.2.3.

2.2.1. Derivation of the ODEs

The 1D cross sectional-integrated continuity and momentum equations for sediment-laden flows can be written as (Dou et al., 2014; Wu and Wang, 2007).

$$\frac{\partial(\rho_m A)}{\partial t}+\frac{\partial(\rho_m Q)}{\partial x}=-\frac{\partial(\rho_s' A_s)}{\partial t} \tag{1}$$

$$\frac{\partial(\rho_m Q)}{\partial t}-\left(\frac{Q^2}{A^2}-gh\right)\frac{\partial(\rho_m A)}{\partial x}+\frac{2Q}{A}\frac{\partial(\rho_m Q)}{\partial x} =\left(\rho_m gh^2\frac{\partial B}{\partial x}+gA(h-h_c)\frac{\partial \rho_m}{\partial x}\right)+(G'-T) \tag{2}$$

where x = streamwise coordinate, t = time; Q = flow discharge; A_s = bed area at cross section; A = flow area; B = river width at the water surface; $h = A/B$ = average flow depth; $h_c \approx 0.5h$ = flow depth at the cross-sectional centroid, with a rectangular cross section being assumed; g = gravitational acceleration; $\rho_m = \rho_w(1-c)+\rho_s c$ = density of the sediment-laden flow; $\rho_s' = \rho_w p + \rho_s(1-p)$ = density of the saturated bed; c = volumetric sediment concentration; ρ_w = water density, ρ_s = sediment density, p = bed sediment porosity; $G' = \rho_m gAJ_b$ = streamwise component of gravity; J_b = bed slope; $T = \rho_m gAJ_f$ = flow resistance; $J_f = n^2(Q/A)^2/h^{4/3}$ = friction slope; n = Manning roughness.

To derive the ODEs (compatibility equations) along the characteristics, Eqs. (1) and (2) are combined together by Eq. (1) × φ + Eq. (2), where φ is a coefficient to be determined later. This results in the following equation:

$$\frac{\partial(\rho_m Q)}{\partial t}+\left(\frac{2Q}{A}+\varphi\right)\frac{\partial(\rho_m Q)}{\partial x}+\varphi\left[\frac{\partial(\rho_m A)}{\partial t}+\frac{1}{\varphi}\left(gh-\frac{Q^2}{A^2}\right)\frac{\partial(\rho_m A)}{\partial x}\right] =C-\varphi\frac{\partial(\rho_s' A_s)}{\partial t} \tag{3}$$

where $C=\rho_m gh^2\frac{\partial B}{\partial x}+gA(h-h_c)\frac{\partial \rho_m}{\partial x}+G'-T$ is related to the river width gradient (i.e., $C_1=\rho_m gh^2\frac{\partial B}{\partial x}$), the flow density gradient (i.e., $C_2=gA(h-h_c)\frac{\partial \rho_m}{\partial x}$), the streamwise component of the gravity and the resis-

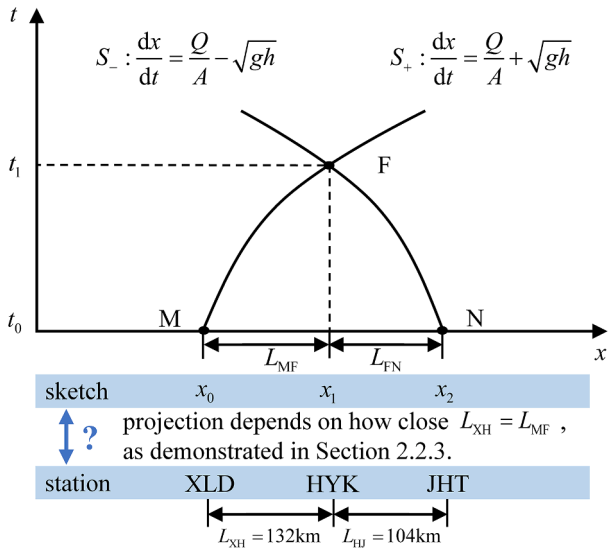

Fig. 3. Sketch of the characteristic method as well as its projection to the three stations in the Lower Yellow River. Two characteristics (S_+, S_-) drawn starting from M (x_0, t_0) and N (x_2, t_0) intersect at F (x_1, t_1). Whether the actual stations (XLD, HYK, JHT) can correspond to the sketch positions (M, F, N) depends on how close the L_{XH} (i.e., 132 km) is to theL_{MF}, as demonstrated in Section 2.2.3.

tance ($C_3 = G' - T$). Assuming $\left(\frac{2Q}{A} + \varphi\right) = \frac{1}{\varphi}\left(gh - \frac{Q^2}{A^2}\right) = \frac{dx}{dt}$ (this requires $\varphi = -\frac{Q}{A} \pm \sqrt{gh}$), Eq. (3) can be rewritten as:

$$\frac{\partial(\rho_m Q)}{\partial t} + \frac{\partial(\rho_m Q)}{\partial x}\frac{dx}{dt} + \left(-\frac{Q}{A} \pm \sqrt{gh}\right)\left[\frac{\partial(\rho_m A)}{\partial t} + \frac{\partial(\rho_m A)}{\partial x}\frac{dx}{dt}\right] = C - \left(-\frac{Q}{A} \pm \sqrt{gh}\right)\frac{\partial(\rho_s' A_s)}{\partial t} \tag{4}$$

Considering the integral rule ($\frac{d\,F(x,\,t)}{dt} = \frac{\partial\,F(x,\,t)}{\partial t} + \frac{\partial\,F(x,\,t)}{\partial x}\frac{dx}{dt}$), Eq. (4) can be rewritten as ODEs (5a) along the characteristics described by Eq. (5b):

$$\frac{d(\rho_m Q)}{dt} + \left(-\frac{Q}{A} \pm \sqrt{gh}\right)\frac{d(\rho_m A)}{dt} = C - \left(-\frac{Q}{A} \pm \sqrt{gh}\right)\frac{\partial(\rho_s' A_s)}{\partial t} \tag{5a}$$

$$\frac{dx}{dt} = \frac{Q}{A} \pm \sqrt{gh} \tag{5b}$$

Thereafter, the propagation of disturbance in the fluvial process in space–time coordinates can be sketched as Fig. 3, where three positions (M at x_0 and t_0, F at x_1 and t_1, N at x_2 and t_0) are highlighted.

Integrating the ODEs (Eq. (5a)) along their corresponding characteristics respectively (Eq. (5b), see Fig. 3) gives:

$$\int_M^F d(\rho_m Q) + \int_M^F \left(-\frac{Q}{A} + \sqrt{gh}\right) d(\rho_m A) = \int_M^F \left[C - \left(-\frac{Q}{A} + \sqrt{gh}\right)\frac{\partial(\rho_s' A_s)}{\partial t}\right] dt \tag{6a}$$

$$\int_N^F d(\rho_m Q) + \int_N^F \left(-\frac{Q}{A} - \sqrt{gh}\right) d(\rho_m A) = \int_N^F \left[C - \left(-\frac{Q}{A} - \sqrt{gh}\right)\frac{\partial(\rho_s' A_s)}{\partial t}\right] dt \tag{6b}$$

Applying to the integral median theorem (that is: $\int_a^b f(x)\,d(g(x)) = [\beta f(a) + (1-\beta) f(b)][g(b) - g(a)]$, where $\beta \in [0,1]$ represents the weighting parameter) and letting $\frac{\partial(\rho_s' A_s)}{\partial t} \approx \frac{\rho_s' \Delta A_s}{\Delta t}$ with ΔA_s being taken as the change of the bed area at cross section during the time interval Δt, Eqs. (6a) and (6b) can be recast into:

$$(\rho_m Q)_F - (\rho_m Q)_M + D_1\left[(\rho_m A)_F - (\rho_m A)_M\right] = E_1 \Delta t + K_1 \tag{7a}$$

$$(\rho_m Q)_F - (\rho_m Q)_N + D_2\left[(\rho_m A)_F - (\rho_m A)_N\right] = E_2 \Delta t + K_2 \tag{7b}$$

where $D_1 = \beta_1\left(-\frac{Q}{A} + \sqrt{gh}\right)_M + (1-\beta_1)\left(-\frac{Q}{A} + \sqrt{gh}\right)_F$,

$D_2 = \beta_2\left(-\frac{Q}{A} - \sqrt{gh}\right)_N + (1-\beta_2)\left(-\frac{Q}{A} - \sqrt{gh}\right)_F$,

Table 2
Expressions of influencing terms in two strategies.

Part	Terms	Physical implication	Expressions in strategy 1	Expressions in strategy 2
1	I	longitudinal flow density change on the upstream discharge	$\left[\frac{(\rho_m)_M}{(\rho_m)_F} - 1\right] Q_M$	$\left[\frac{(\rho_m)_M}{(\rho_m)_F} - 1\right] Q_M$
2	II	longitudinal change of $\rho_m A$ derived from advection and pressure term	$\frac{D_1}{(\rho_m)_F}[(\rho_m A)_M - (\rho_m A)_F]$	$\frac{1}{(\rho_m)_F}\frac{D_1 D_2}{D_2 - D_1}[(\rho_m A)_M - (\rho_m A)_N]$
3	III	temporal cumulative effect of pressure term caused by river width gradient	$\frac{\Delta t}{(\rho_m)_F}[\beta_1 (C_1)_M + (1-\beta_1)(C_1)_{F+}]$	$\frac{\Delta t}{(\rho_m)_F}\left\{\frac{[\beta_1 (C_1)_M + (1-\beta_1)(C_1)_{F+}]D_2' + [\beta_2 (C_1)_N + (1-\beta_2)(C_1)_{F-}]D_1}{D_2' + D_1}\right\}$
	IV	temporal cumulative effect of pressure term caused by flow density gradient	$\frac{\Delta t}{(\rho_m)_F}[\beta_1 (C_2)_M + (1-\beta_1)(C_2)_{F+}]$	$\frac{\Delta t}{(\rho_m)_F}\left\{\frac{[\beta_1 (C_2)_M + (1-\beta_1)(C_2)_{F+}]D_2' + [\beta_2 (C_2)_N + (1-\beta_2)(C_2)_{F-}]D_1}{D_2' + D_1}\right\}$
	V	temporal cumulative effect of external force including gravity and resistance	$\frac{\Delta t}{(\rho_m)_F}[\beta_1 (C_3)_M + (1-\beta_1)(C_3)_{F+}]$	$\frac{\Delta t}{(\rho_m)_F}\left\{\frac{[\beta_1 (C_3)_M + (1-\beta_1)(C_3)_{F+}]D_2' + [\beta_2 (C_3)_N + (1-\beta_2)(C_3)_{F-}]D_1}{D_2' + D_1}\right\}$
	VI	effect of momentum term due to bed deformation	$\frac{K_1}{(\rho_m)_F}$	$\frac{1}{(\rho_m)_F}\left(\frac{K_1 D_2' + K_2 D_1}{D_2' + D_1}\right)$
4	VII	effect of imbalanced advection	/	$\frac{1}{(\rho_m)_F}\frac{D_1}{D_2 - D_1}[(\rho_m Q)_M - (\rho_m Q)_N]$

Note: In this table, expressions of terms are rewritten by substituting the coefficient of each parts (i.e., $\alpha_1 \sim \alpha_3$ in strategy 1, $\alpha_1 \sim \alpha_4$ in strategy 2). The key factors in term III ~ V are involved in $C_1 = \rho_m g h^2 \frac{\partial B}{\partial x}$, $C_2 = gA(h - h_c)\frac{\partial \rho_m}{\partial x}$, $C_3 = G' - T$, and ΔA_s involved in K_1 and K_2 for term VI. Additionally, term VI in strategy 2 can be rewritten in the form related to the longitudinal variation of ΔA_s in M−F, N−F, and M−N reach:
$\frac{1}{(\rho_m)_F(D_2' + D_1)}\left\{\rho_s'\beta(1-\beta)(-\frac{Q}{A} + \sqrt{gh})_M(\frac{Q}{A} + \sqrt{gh})_F[(\Delta A_s)_F - (\Delta A_s)_M] + \rho_s'\beta(1-\beta)(\frac{Q}{A} + \sqrt{gh})_N(-\frac{Q}{A} + \sqrt{gh})_F[(\Delta A_s)_N - (\Delta A_s)_F] + \rho_s'\beta^2(-\frac{Q}{A} + \sqrt{gh})_M(\frac{Q}{A} + \sqrt{gh})_N[(\Delta A_s)_N - (\Delta A_s)_M]\right\}$, where β indicates the value of the weighting parameter, i.e., $\beta_1 = \beta_2$.

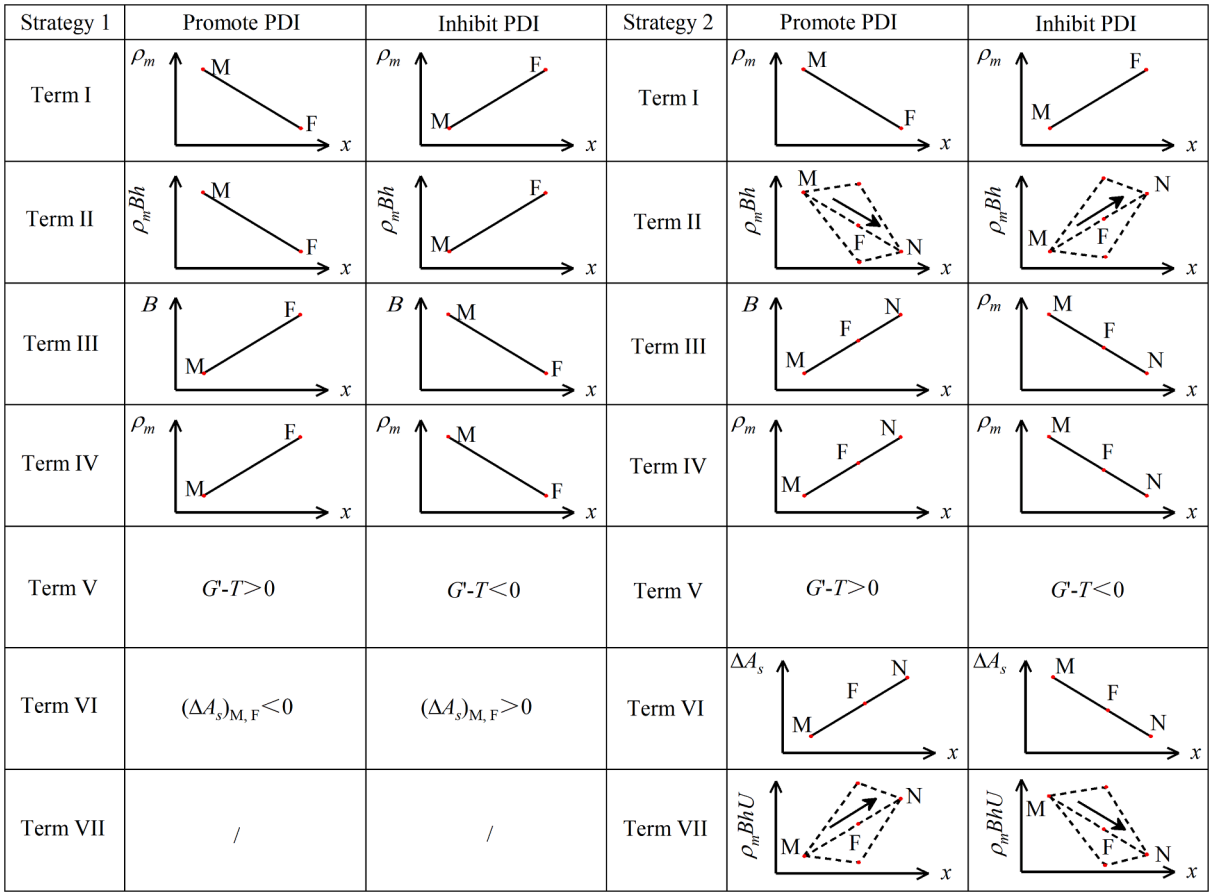

Fig. 4. Sketch of effecting mechanisms of critical factors on PDI. The subscript of ΔA_s in strategy 1 denotes the bed area simultaneously change at M and F. It is noted that the influence of the ΔA_s in strategy 2 is established under the condition that $\beta_1 = \beta_2$.

$$E_1 = \beta_1 C_M + (1-\beta_1)C_{F+},\ E_2 = \beta_2 C_N + (1-\beta_2)C_{F-},$$
$$K_1 = -\left\{\beta_1\left[\left(-\frac{Q}{A}+\sqrt{gh}\right)\rho_s'\Delta A_s\right]_M + (1-\beta_1)\left[\left(-\frac{Q}{A}+\sqrt{gh}\right)\rho_s'\Delta A_s\right]_F\right\},$$
$$K_2 = -\left\{\beta_2\left[\left(-\frac{Q}{A}-\sqrt{gh}\right)\rho_s'\Delta A_s\right]_N + (1-\beta_2)\left[\left(-\frac{Q}{A}-\sqrt{gh}\right)\rho_s'\Delta A_s\right]_F\right\},$$

In the expressions of E_1 and E_2, distinct values of C at F (i.e., C_{F+} and C_{F-}) are involved. It is because: 1) the parameter C contains spatial gradients of the river width and flow density, and 2) the longitudinal variation features of the river width and the flow density may be different along the two characteristics. In the above parameters, $\beta_1 \in [0, 1]$ and $\beta_2 \in [0, 1]$ represent the weighting parameters for the relative contribution of M in the M−F reach and of N in the N−F reach, respectively.

2.2.2. Strategies for using the ODE of discharge variation

There can be two strategies to use Eq. (7)to attain the flow discharge at F. The most straightforward strategy (strategy 1) is only to use Eq. (7a), from which a relation of peak discharges between M and F can be obtained in the following:

$$Q_F = Q_M + \underbrace{\frac{\alpha_1 Q_M}{\text{Part 1}}}_{\text{Part 1}} + \underbrace{\frac{\alpha_2[(\rho_m A)_M - (\rho_m A)_F]}{\text{Part 2}}}_{\text{Part 2}} + \underbrace{\frac{\alpha_3 \Delta t}{\text{Part 3}}}_{\text{Part 3}} \tag{8}$$

where $\alpha_1 = \frac{(\rho_m)_M}{(\rho_m)_F} - 1$, $\alpha_2 = \frac{D_1}{(\rho_m)_F}$, $\alpha_3 = \frac{1}{(\rho_m)_F}\left(E_1 + \frac{K_1}{\Delta t}\right)$.

From Eq. (8), the discharge at F is dictated by the discharge at M and three additional parts (Part 1, Part 2, and Part 3). As shown in Table 2, Part 1 ~ 2 involve only one influencing term, respectively (i.e., I in Part 1 and II in Part 2). While Part 3 can be further divided into four influencing terms (III ~ VI) by the substitution of the expressions of E_1 and K_1. All these terms have the dimension of L^3/T. Following the expressions of the six influencing terms in Table 2 (see the forth column), one can readily deduce their effects on PDI from a qualitative perspective, which lead to Fig. 4.

Term I is the product of the coefficient α_1 and the discharge at M. Since the discharge at M is always positive, the α_1 value determines the role of term I. Since $\alpha_1 = \frac{(\rho_m)_M}{(\rho_m)_F} - 1$, term I represents the effect of the longitudinal flow density change on the PDI. Considering that the flow density depends directly on sediment concentration, a longitudinal decreasing sediment concentration means $\alpha_1 > 0$, and vice versa. Consequently, longitudinal decreasing sediment concentration would promote PDI, whereas a longitudinal increasing sediment concentration would attenuate PDI.

Term II is the product of the coefficient α_2 and the longitudinal variation of $\rho_m A$ (i.e., $\rho_m Bh$) in the M−F reach, where the coefficient α_2 depends on D_1. Given that the flow in Yellow River is always subcritical (e.g., $\sqrt{gh} > \frac{Q}{A}$), it can be easily proved that D_1 is always positive. Consequently, α_2 would be always positive. Therefore, it is the longitudinal variation of the product $\rho_m A$ that determines the effect of term II on the PDI. It is appreciated that a longitudinal decreasing $\rho_m A$ would promote PDI, and in contrast, a longitudinal increasing $\rho_m A$ would attenuate PDI.

Terms III ~ VI are included in Part 3, reflecting the accumulated effects of four factors. The cumulative effects of pressure term due to the longitudinal river width gradient and the longitudinal flow density gradient are involved in terms III and IV, respectively. From the expression of term III, it is apparent that ρ_m, Δt, g, h are always positive, and accordingly, the effect of term III is dictated by the critical parameter $\frac{\partial B}{\partial x}$. Apparently, a positive $\frac{\partial B}{\partial x}$ leads to a positive term III and the reverse a negative value. In other words, an increasing river width in the streamwise direction would facilitate PDI, and vice versa. Likewise,

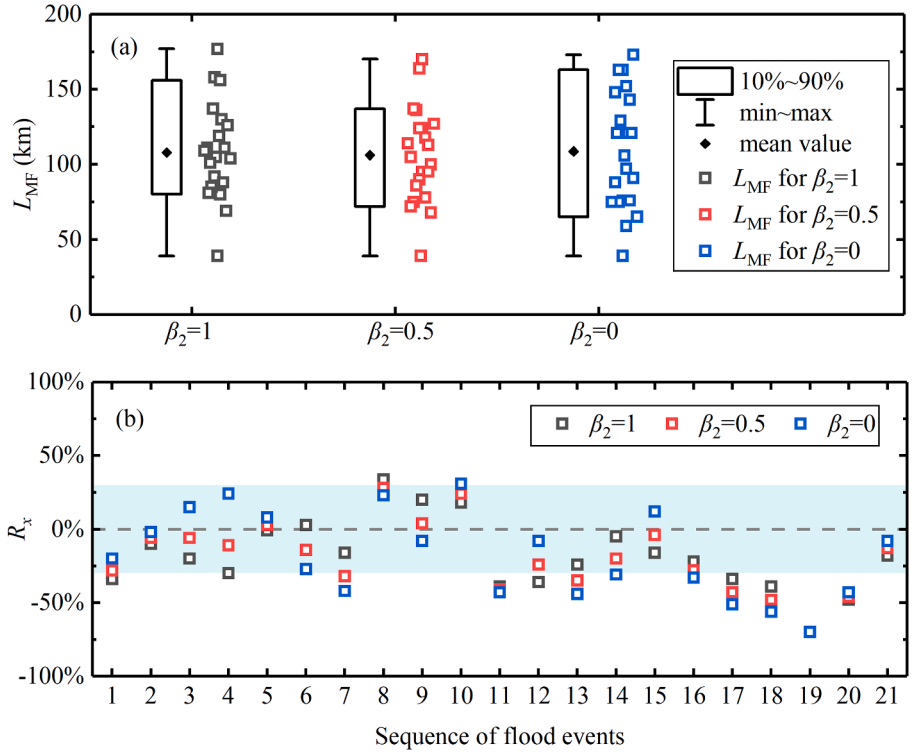

Fig. 5. (a) Boxplot of the calculated value of L_{MF} (the calculated values are shown to the side as gray, red, and blue dots which correspond to the value of L_{MF} with β_2 taking 1, 0.5, and 0, respectively), and (b) relative deviation of the L_{MF} from theL_{XH}. The blue shaded area indicates the interval with deviation less than 30 %, i.e., $|R_x| < 30$ %.

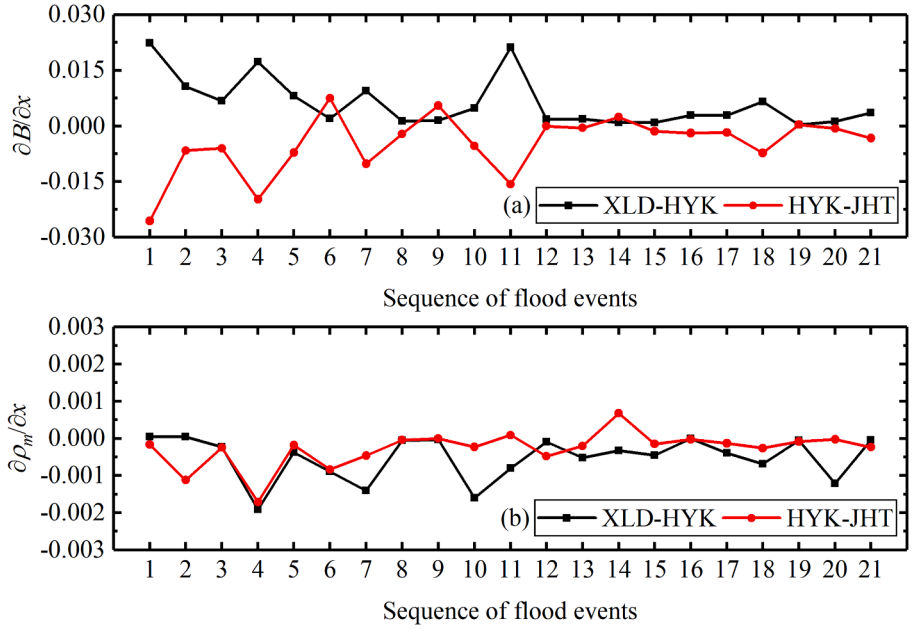

Fig. 6. (a) The gradients of river width, and (b) the flow density gradient at different reaches in each flood event.

the effect of term IV depends on the critical factor $\frac{\partial \rho_m}{\partial x}$ as other parameters (ρ_m, Δt, g, h, h_c, A) involved in its expression are always positive. Therefore, a longitudinal increasing flow density would promote PDI, whereas a longitudinal decreasing flow density would attenuate PDI. Term V is related to the cumulative effects of external force composed of gravity and resistance. It is recognized that the relative strength of the two forces determines the effect of term V because other parameters (ρ_m, Δt) are positive in the expression. When the gravity is greater than the resistance (i.e., $G' - T > 0$), term V would promote PDI, and vice versa. Term VI reflects the effect of the momentum term due to the bed deformation. The expression of K_1 constituting term VI predominately involves two parts, i.e., the product of $(-\frac{Q}{A} + \sqrt{gh})$, ρ_s', ΔA_s at M and F respectively, and the weighting parameter β_1 determines their respective magnitudes. Since $(-\frac{Q}{A} + \sqrt{gh})$ and ρ_s' are always positive, the effect

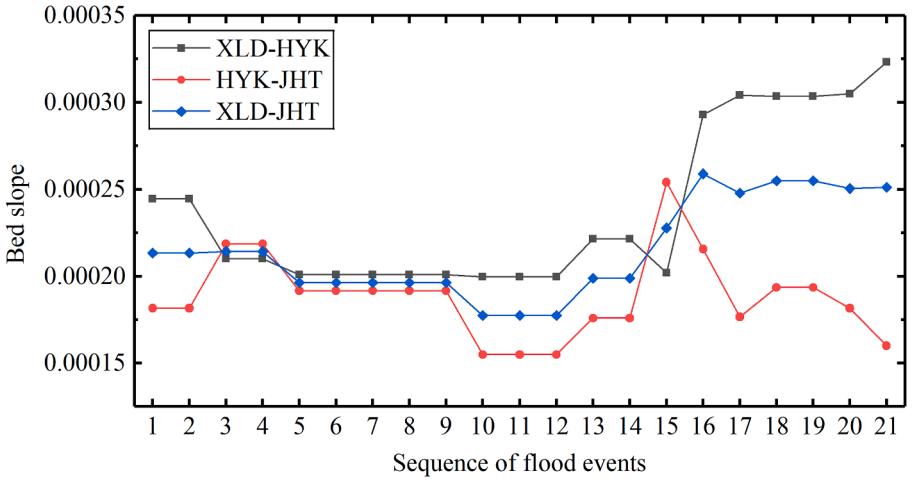

Fig. 7. Bed slope of XLD−HYK, HYK−JHT and XLD−JHT reach before flood.

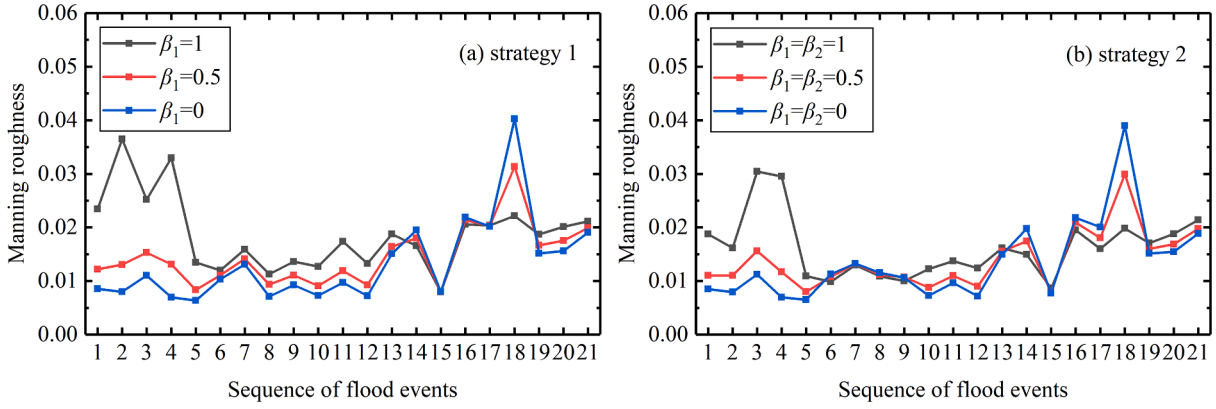

Fig. 8. The back-estimated value of Manning roughness. (a) strategy 1, (b) strategy 2. The rough range of Manning roughness documented by YRCC is 0.004 ~ 0.058.

of term VI is dictated by the change of bed area (ΔA_s). It follows that the simultaneous bed degradation (i.e., $\Delta A_s < 0$) at both the two neighbouring stations would promote PDI, and vice versa. Obviously, it is hard to determine the effect of term VI, given the inconsistent bed deformation (deposition or erosion) at the two stations. Under this condition, one has to take the value of β_1 and the bed deformations of two stations into account to deduce the effect of term VI.

The second strategy uses both Eq. (7a) and (7b) by the mathematical manipulation: Eq.(7b) × D_1 −Eq.(7a) × D_2, from which a relation of peak discharges among M, N and F can be obtained in the following:

$$Q_F = Q_M + \underbrace{\frac{\alpha_1 Q_M}{\text{Part 1}}} + \underbrace{\frac{\alpha_2[(\rho_m A)_M - (\rho_m A)_N]}{\text{Part 2}}} + \underbrace{\frac{\alpha_3 \Delta t}{\text{Part 3}}} + \underbrace{\frac{\alpha_4[(\rho_m Q)_M - (\rho_m Q)_N]}{\text{Part 4}}} \tag{9}$$

where $\alpha_1 = \frac{(\rho_m)_M}{(\rho_m)_F} - 1$, $\alpha_2 = \frac{1}{(\rho_m)_F}\frac{D_1 D_2}{D_2 - D_1}$, $\alpha_3 = \frac{1}{(\rho_m)_F}\left[\left(\frac{E_1 D_2 - E_2 D_1}{D_2 - D_1}\right) + \left(\frac{K_1 D_2 - K_2 D_1}{D_2 - D_1}\right)\frac{1}{\Delta t}\right]$, $\alpha_4 = \frac{1}{(\rho_m)_F}\frac{D_1}{D_2 - D_1}$.

From Eq. (9), the discharge at F depends on the discharge at M and four additional parts (Part 1 ~ 4), where the effects of the discharge at N are involved. Four influencing terms (III ~ VI) constitute Part 3, while only one influencing term for the other parts (i.e., I in Part 1, II in Part 2, and VII in Part 4). All terms here also have the same dimension of L^3/T. A total of seven influencing terms (I ~ VII) defined in this strategy are shown in Table 2 (see the fifth column), from which their qualitative performance also is illustrated in Fig. 4.

Term I obtained here is the same as that in strategy 1, associated with the longitudinal change of flow density in the M−F reach. As deduced above, a longitudinal decreasing sediment concentration would promote PDI, and the reverse would attenuate PDI.

Term II is the product of the coefficient α_2 and the difference of $\rho_m A$ (i.e., $\rho_m Bh$) between M and N, in which the coefficient α_2 is determined by both D_1 and D_2. It can be proved that α_2 is invariably positive due to the positive value of D_1 and the negative value of D_2 given the subcritical flow (e.g., $\sqrt{gh} > \frac{Q}{A}$). Accordingly, the effect of term II depends on the difference of $\rho_m A$. Irrespective of the change of the middle reach, it is appreciated that a decreasing $\rho_m A$ directed from M to N would promote PDI, whereas an increasing $\rho_m A$ would inhibit PDI (see Fig. 4).

It is similar to strategy 1, terms III ~ VI constitute Part 3 reflecting the accumulated effects related to the four key factors (i.e., $\frac{\partial B}{\partial x}$, $\frac{\partial \rho_m}{\partial x}$, $G' - T$, ΔA_s). However, the qualitative performances of the four terms are not identical to that in strategy 1 because the expressions are more complicated (see the fifth column in Table 2), taking into account the impact of the F−N reach. Specifically, positive parameters D_1 and $D_2' = -D_2$ are introduced in terms III ~ VI. Following the expressions of terms III ~ V, their effects are directly determined by $\frac{\partial B}{\partial x}$, $\frac{\partial \rho_m}{\partial x}$, $G' - T$ due to other parameters (ρ_m, Δt, g, h, h_c, A) are always positive. For terms III and IV, a monotonically increasing trend of the key factor in the streamwise direction would promote PDI, and vice versa. For term V, $G' - T > 0$ would promote PDI, while $G' - T < 0$ would inhibit PDI. The effect of term VI depends on $K_1 D_2' + K_2 D_1$, where K_1 involves the bed deformation at M and F affected by β_1, and K_2 involves the bed deformation at N and F affected by β_2. It is difficult to determine the sign of term VI due to the complicated components in the expression, which

Trends		flow density	river width	water depth	bed deformation	flow discharge
Monotonic change	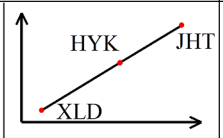	/	Nos.6,9,14,19	/	Nos.3,4,16,21	/
	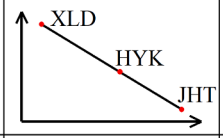	Nos.3~10,12, 13,15~21	/	Nos.6~11,13, 16,17	Nos.15,18,19	/
Nonmonotonic change XLD-HYK: increasing HYK-JHT: decreasing	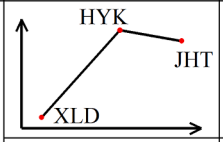	/	Nos.1~5,7,10~13, 16~18,20,21	/	Nos.1,2,5~9,17	Nos.2,19,20
	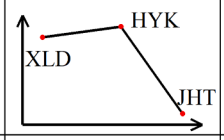	Nos.1,2	Nos.8,15	Nos.14,15,18,19	/	Nos.1,3~18,21
Nonmonotonic change XLD-HYK: decreasing HYK-JHT: increasing	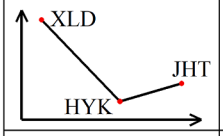	No.11	/	Nos.1~5,12,20,21	Nos.10~14,20	/
	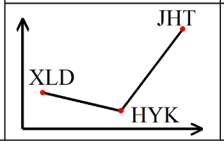	No.14	/	/	/	/

Fig. 9. Variation trends sketch of filed data. Totally-six trends of measured physical factors (ρ_m, B, h, ΔA_s, Q) including monotonic and non-monotonic variation from XLD station to HYK station then to JHT station are summarized in this figure.

prevent a qualitative understanding for term VI. Given $\beta_1 = \beta_2$, the complicated expression can be simplified as the sum of three parts related to the longitudinal variation of ΔA_s in the M−N, M−F, and F−N reach (as shown in the notes of Table 2). This provides an approach to clarify how the term VI is affected by bed deformation and facilitates the qualitative understanding of term VI. Accordingly, the longitudinal variation of ΔA_s is used to predict the effect of term VI, i.e., a monotonically increasing ΔA_s would promote PDI, whereas a monotonically decreasing ΔA_s would attenuate PDI. It is different from strategy 1, in which the ΔA_s at M and F (i.e., erosion or deposition) are directly used to predict the effect of term VI.

It is also noted that the effects of terms III ~ VI are difficult to be determined qualitatively in the case of non-monotonic variation along the M−F−N reach. Alternatively, their impacts may depend on the dominant reach.

Apart from the above influencing terms, an additional term VII in Part 4 representing the influence of imbalanced advection transport between upstream and downstream is also considered. Term VII is the product of a coefficient α_4 and the difference of $\rho_m Q$ (i.e., $\rho_m BhU$) between M and N. The α_4 is invariably negative with a positive D_1 and a negative D_2, and thus term VII is determined by the difference of $\rho_m Q$. Accordingly, an increasing $\rho_m Q$ would promote PDI, whereas a decreasing $\rho_m Q$ would attenuate PDI.

2.2.3. Correspondence between M−F−N and XLD−HYK−JHT

Before applying the discharge equation (either strategy 1 or strategy 2), one should check whether the three stations (XLD, HYK, and JHT) can have a similar relation as M−F−N shown in Fig. 3. Under the assumption that the correspondence between XLD−HYK−JHT and M−F−N is established, the following relations are required:

$$\frac{x_1 - x_0}{t_1 - t_0} = \beta_1 \left(\frac{Q}{A} + \sqrt{gh}\right)_{\mathrm{XLD}} + (1-\beta_1)\left(\frac{Q}{A} + \sqrt{gh}\right)_{\mathrm{HYK}} \tag{10a}$$

$$\frac{x_1 - x_2}{t_1 - t_0} = \beta_2 \left(\frac{Q}{A} - \sqrt{gh}\right)_{\mathrm{JHT}} + (1-\beta_2)\left(\frac{Q}{A} - \sqrt{gh}\right)_{\mathrm{HYK}} \tag{10b}$$

For Eq. (10), we can take $x_1 - x_0$ (i.e., L_{MF} in Fig. 3) as an unknown, which can be back-estimated from other parameters using measured data at the three stations. The discrepancy between the calculated L_{MF} and the actual distance from XLD to HYK (i.e., $L_{\mathrm{XH}} = 132$ km) would indicate whether the three stations have a similar relation as M−F−N.

However, flood wave propagation in the LYR is very complex, from inside the channel to overflowing on the floodplain, from relatively narrow-deep to wide-shallow channel. It is therefore inaccurate to directly adopt the characteristic celerity for estimation. As a compromise, the characteristic celerity along the S_+ characteristics (the right-hand side of Eq.(10a)) is replaced by the following estimation: $\frac{L_{\mathrm{XH}}}{\Delta t_i}$, where Δt_i is the actual time interval for peak discharge propagation from XLD to HYK (see the last column in Table 1). In addition, it is necessary to specify the β_2 value for calculating L_{MF}. Here we tentatively take three values (1, 0.5, 0) as examples. Fig. 5**a** shows the range of calculated L_{MF} with different β_2. On average, the calculated value of L_{MF} is 108 km, 106 km, and 109 km, against the β_2 value of 1, 0.5, and 0, respectively. Fig. 5**b** shows the relative deviation of the calculated distance (L_{MF}) from the actual distance between XLD and HYK (L_{XH}), which is defined as $R_x = (L_{\mathrm{MF}} - L_{\mathrm{XH}})/L_{\mathrm{XH}}$. From Fig. 5**b**, there are approximately two-thirds of floods with $|R_x| < 30$ % (the area highlighted by blue shading).

Indeed, inevitable discrepancies arise in the above calculation. This is because a more accurate result requires a very small distance between

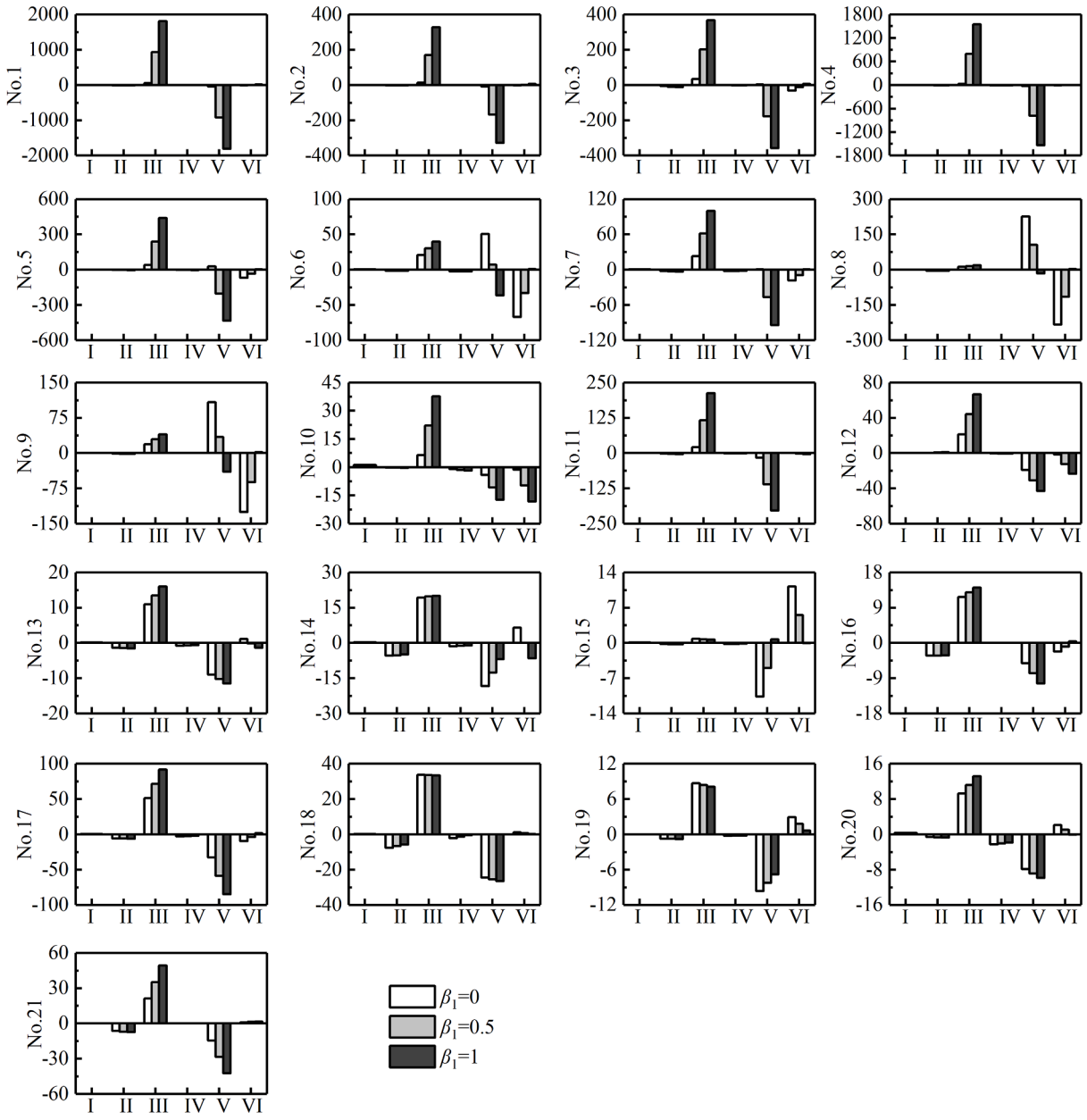

Fig. 10. Estimated values of each influencing term normalized by the discharge increment for strategy 1.

M and N in Fig. 3, based on the assumption that the disturbance propagates at a constant celerity. However, the hydrological survey is carried out only at the three adjacent stations (XLD, HYK, and JHT) along the river. There are no other stations in-between, and the next station is Gaocun, which is 70 km downstream of JHT station. Accordingly, in the absence of more available data for the LYR, it is advisable to assume M, F, and N as XLD, HYK, and JHT stations, respectively.

3. Results

3.1. Validation of the back-estimated roughness

Prior to proceeding to estimate, the following parameters are specified as: $\rho_w = 1000$ kg/m^3, $\rho_s = 2650$ kg/m^3, $p = 0.45$ by referring to the Yellow River background. Parameters from the decomposition of each term in Eqs. (8-9) can be categorized into four types (i.e., type 1 ~ 4). Values of parameters in type 1 have been documented (e.g., Q, A) or can be readily computed (e.g., h, h_c, ρ_m, ρ_s', $\Delta t = \Delta t_i$ and ΔA_s = the difference in the cross-sectional area of the bed above a reference datum before and after the flood season, see Table 1) from the documented data in Table 1 (i.e., Q, A, B, c) and the parameters that have been specified above (i.e., ρ_w, ρ_s, p). Values of parameters in type 2 (e.g., $\frac{\partial B}{\partial x}$, $\frac{\partial \rho_m}{\partial x}$, J_b) can be computed from type 1 parameters using linear assumption. Among type 2 parameters, $\frac{\partial B}{\partial x}$ and $\frac{\partial \rho_m}{\partial x}$ are concerned about the spatial gradients of the river width and the flow density, and the values of which in the XLD−HYK and HYK−JHT reach are used at XLD and JHT, respectively. While $\frac{\partial B}{\partial x}$ and $\frac{\partial \rho_m}{\partial x}$ at HYK depend on which one of the characteristics follows along, i.e., the XLD−HYK reach is used at HYK for the S_+ characteristics, whereas the HYK−JHT reach for the S_- characteristics (see Fig. 6). Fig. 7 shows the values of J_b, which are estimated by the longitudinal gradient of the bed elevation of the thalweg. It exhibits the appreciable difference between the upstream (XLD−HYK reach) and the downstream (HYK−JHT reach) of the HYK station, that is, the upstream reach (black line) is steeper than the downstream reach (red line) in most floods. To accurately describe this feature, the bed slopes of the

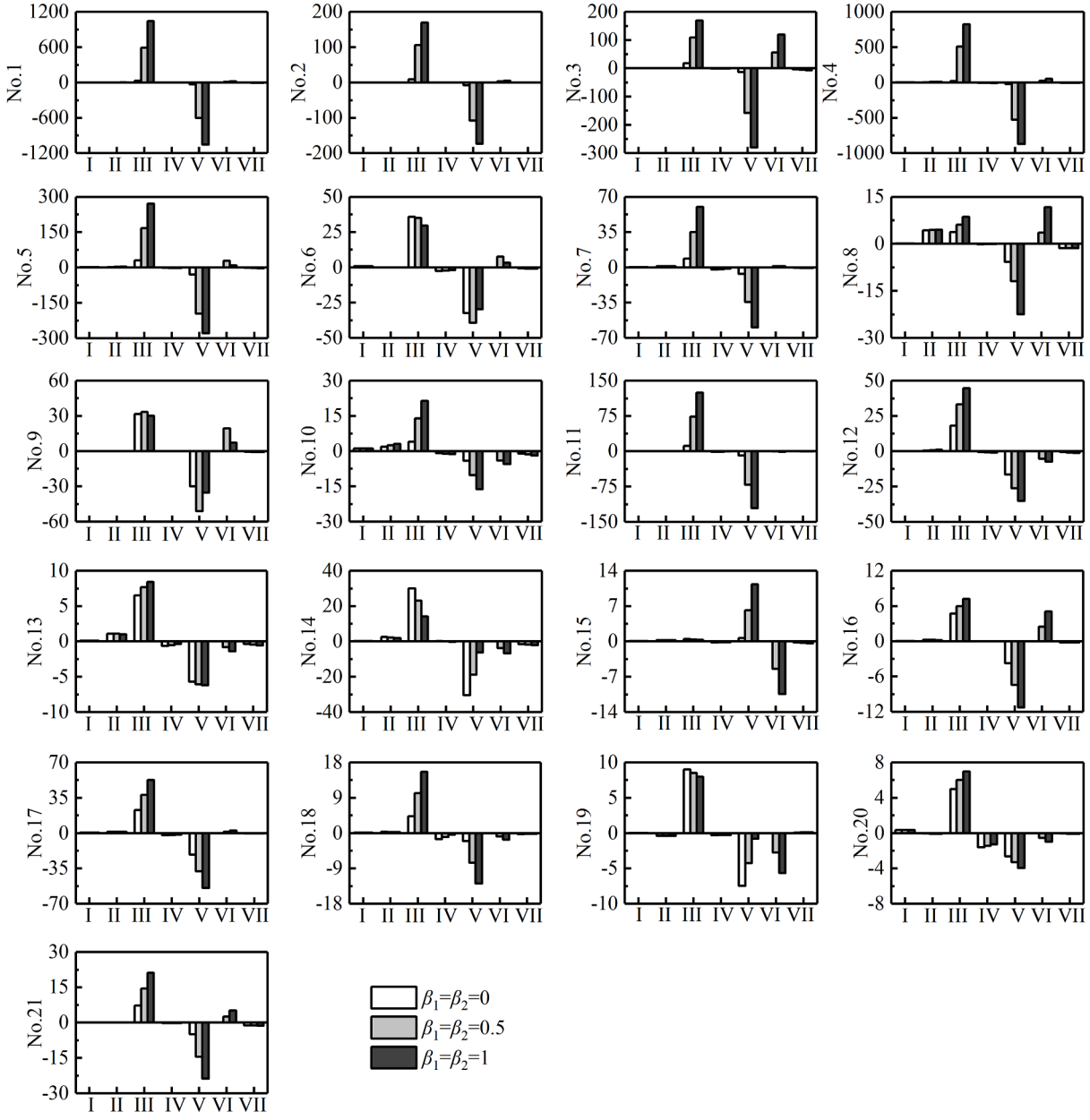

Fig. 11. Estimated values of each influencing term normalized by the discharge increment for strategy 2.

XLD−HYK reach and the HYK−JHT reach are adopted at XLD and JHT, respectively. In particular, the bed elevation gradient in the XLD−JHT reach is used at the HYK station. It is noted that the filed data of bed elevation at the XLD station before 2006 are missing. And thus, the data at the closest Tiexie station is used as a replacement. Values of parameters in type 3 (i.e., β_1, β_2) must be specified manually, and three values (1, 0.5, 0) are tentatively used here. In addition, for the values of Manning roughness (i.e., n) in type 4, there is no systematically-documented data, but a rough range of which can be given from rare measured data. Therefore, it is proposed here to back calculate the Manning roughness from parameters of types 1 ~ 3. Afterwards, the back-calculated bed roughness is compared to the documented range, of which the discrepancy is adopted as an indicator for the reasonableness of the present method. Of particular note is that the bed material and bedform also considerably affect the roughness value. For instance, bed incisions accompanied by sediment coarsening after damming and the change of bed topography facilitate the development of large dunes, which contribute to the increase of flow resistance (Ma et al., 2022). All these impacts are incorporated into the back-calculated roughness value in the present study.

Fig. 8 shows the back-calculated Manning roughness in strategy 1 and strategy 2, where three scenarios are conducted in both strategies. Specifically, β_1=1, 0.5, and 0 are used in strategy 1. For convenience in analysis, assuming $\beta_1 = \beta_2$ in strategy 2, and also three values (1, 0.5, 0) are used. In strategy 1, the roughness varies in 0.007 ~ 0.036, 0.008 ~ 0.031 and 0.006 ~ 0.04 with the average roughness of 0.019, 0.015 and 0.013 corresponding to $\beta_1 = 1$, 0.5, and 0, respectively. In strategy 2, the average Manning roughness are 0.016, 0.014 and 0.014 whose variation ranges are 0.009 ~ 0.03, 0.008 ~ 0.03 and 0.009 ~ 0.039, corresponding to $\beta_1 = \beta_2 = 1$, 0.5, and 0, respectively. It is appreciated that a larger roughness value is observed in No.2,3,4,18 floods. This is because of the relatively larger water depth (or flow area) in these floods, which leads to a larger C_1 in No.2,3,4 floods when weighting parameters (β_1, β_2) take 1, or a larger G' in No.18 flood when weighting parameters (β_1, β_2) take 0 or 0.5. These differences contribute to a large magnitude of parameter T ($T = C_1 + C_2 + G' - C$) and therefore obtain a

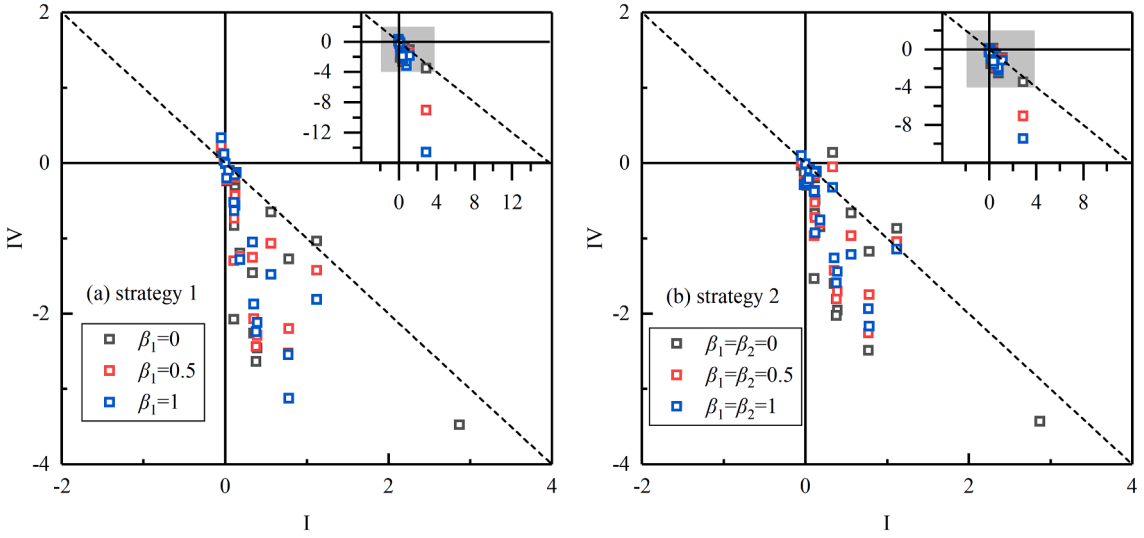

Fig. 12. Values of term I and IV in (a) strategy 1 and (b) strategy 2. The horizontal axis and vertical axis represent the value of term I and IV, respectively. In Fig. 12a, all data points are located at the second quadrant or the fourth quadrant, indicating term I and term IV are always opposite. It is not as so in Fig. 12b.

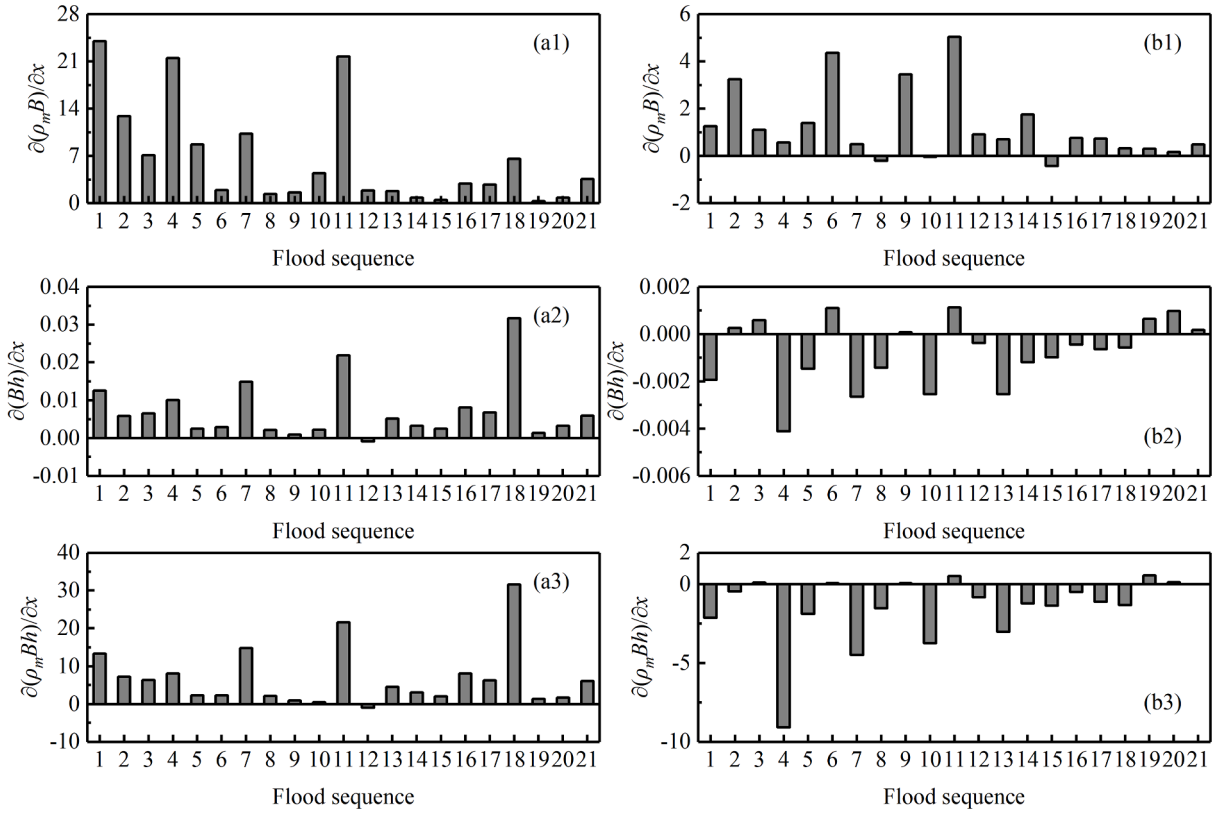

Fig. 13. The variation of $\rho_m B$, Bh, $\rho_m Bh$ between upstream and downstream stations. (a1-a3) longitudinal variation between XLD and HYK station, (b1-b3) longitudinal variation between XLD and JHT station, where a positive value of physical quantity means increasing and the reverse means decreasing.

comparatively large roughness value ($T = \rho_m g A J_f$, $J_f = n^2(Q/A)^2/h^{4/3}$). Numerical uncertainties are inevitable due to simplified assumptions of complex parameters during calculation (e.g., linear assumptions for parameters in type 2). Although the roughness values in these floods exhibit deviations from most floods, they are appreciable only in specific weighting parameters. Nevertheless, all the back-calculated roughness values are almost entirely within the rough range of previously documented results by the YRCC (0.004 ~ 0.058). The reasonably good agreement between the back-calculated roughness and the documented data proves the applicability of the ordinary equations for describing the downstream variation of peak discharge.

3.2. *Performance of influencing terms*

In this section, both the qualitative analysis of influencing terms and the quantitative results of 21 actual floods are employed to reveal insights into the physical mechanism of PDI. Specifically, Fig. 9 shows the actually longitudinal change of some key factors (ρ_m, B, h, ΔA_s, Q) from

the observed data, which is prepared to figure out the qualitative performances of influencing terms in 21 floods. The longitudinal variation of field data involves six trends given the monotonicity of the longitudinal trend and the relative magnitude of XLD and JHT. Both monotonic trend and non-monotonic trend are observed for the longitudinal change of flow density, river width, water depth, and bed deformation at the XLD−HYK−JHT reach, relative to the non-monotonic variation of flow discharge that always increases in the XLD−HYK reach and decreases in the HYK−JHT reach. For strategy 1, it is available to obtain the qualitative performances of terms I, III, IV by corresponding the actual trends of the flow density, river width in the XLD−HYK reach to the theoretical analysis in Fig. 4. Similarly, the qualitative performances of terms I, III, IV, VI in strategy 2 can be determined by the consistency between the monotonic trends of flow density, river width, bed deformation at the XLD−HYK−JHT reach and that in Fig. 4. However, the qualitative effects of terms II, VII is extremely hard to predict directly because the synchronous consideration of multiple factors is necessitated (ρ_m, B, h are involved in term II, and ρ_m, Q are involved in term VII). Apart from this, the qualitative performances of the influencing terms dictated by a non-monotonic variation in strategy 2 are also unpredictable. The quantification appears to be an imminent step towards revealing enhanced understanding of PDI, in recognition the fact that the uncertainty of the effects for influencing terms may remain if only analyse from a qualitative perspective. Hence, the seven influencing terms are further quantified by documented data. To better compare their influence, each term is divided by the discharge increment, and the results are shown in Fig. 10 (strategy 1) and Fig. 11 (strategy 2). From Figs. 10-11, three types of factors that affect PDI are identified as: promoting factors, inhibiting factors and uncertain factors, which are discussed in detail below. For convenience, results relating to $\beta_1 = \beta_2 = 1$ is used for discussion, whereas the influence of β_1, β_2 is discussed in Section 4.

3.2.1. *Promoting factors*

3.2.1.1. Pressure term due to the river width gradient. Term III is the pressure term due to the gradient of river width, which is always positive in Fig. 10. From a qualitative sense, the effect of term III in strategy 1 depends on the longitudinal variation of river width in the XLD−HYK reach. It is recognized that a longitudinal increasing river width would promote PDI (see Fig. 4). Not surprisingly, appreciable increases of the river width from XLD to HYK station are observed in all the 21 floods (see Fig. 9) confirming the promoting effect of term III. Also in Fig. 10, the much greater magnitude of term III further illustrates the dominant role of term III in promoting PDI from a quantitative sense. In strategy 2, term III is closely related with the longitudinal variation of river width in the XLD−HYK−JHT reach. Qualitatively, term III would promote PDI when the river width monotonically increases in the streamwise direction, and vice versa (see Fig. 4). Yet, as shown in Fig. 9, the river width monotonically increases only in 4 floods (Nos.6,9,14,19), while it always increases along XLD−HYK reach but decreases along HYK−JHT reach in the rest floods. Interestingly, it is seen in Fig. 11 that term III is invariably positive in 21 floods. It is apparent that the promoting effect due to a positive term III still prevails in each flood. This indicates the increasing river width in the XLD−HYK reach appears to be more dominant for these non-monotonic circumstances. From a quantitative sense, term III is still prevailing with a relatively appreciable magnitude, which is the largest in 9 floods (Nos.7,10~14,18~20) and the second largest in 11 floods (Nos.1~6,9,15~17,21).

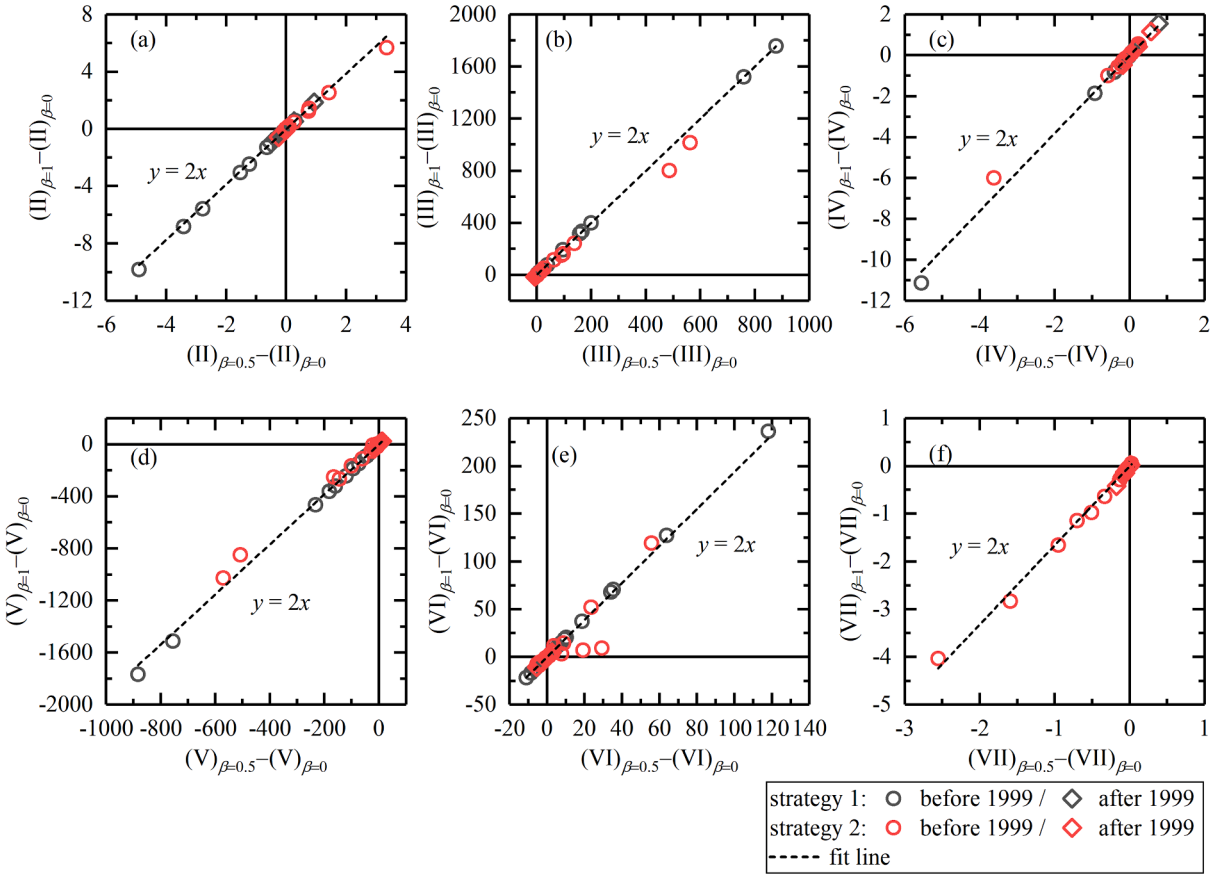

Fig. 14. Effects of weighting parameter on estimation of influencing terms, which is illustrated by comparing $(X)_{\beta=1}-(X)_{\beta=0}$ against $(X)_{\beta=0.5}-(X)_{\beta=0}$, where X represents different terms (II, III, IV, V, VI, VII), and the subscript of X indicates the values of the weighting parameter.

3.2.2. Inhibiting factors

3.2.2.1. External force term. Term V is the external force term that comprises gravity and resistance, whose effects is determined by the relative strength of gravity and resistance. It is seen in Fig. 10 and Fig. 11 that term V is negative in nearly 20 floods (except No.15) in both strategies, indicating that the resistance prevails and it is greater than gravity in most floods. Accordingly, the greater magnitude of negative term V is evoked by the prevailing of the resistance. In strategy 1, term V is a secondary influencing factor relative to term III for most floods from a quantitative sense (except Nos.2,10,15). While in strategy 2, term V is the most dominant in 12 floods (Nos.1~6,8,9,15,17,21), and it is subdominant for other 9 floods. These all demonstrate the external force term plays the paramount role in attenuating the PDI.

3.2.2.2. Longitudinal decreasing flow density. The influence of longitudinal flow density change is incorporated both in term I and term IV. The former reflects the effect of density variation on upstream flow discharge, and the latter is the pressure term due to the longitudinal density gradient. A unique feature is obvious according to the qualitative analysis of strategy 1 (see Fig. 4), that is, as the flow density decreases longitudinally in the M−F reach, term I promotes PDI but term IV attenuates PDI, and vice versa. It is seen from Fig. 9 that the flow density decreases in the XLD−HYK reach in 19 floods (except Nos.1,2 floods). Consequently, one can readily infer that term I promotes PDI and term IV attenuates PDI is prevalent. Yet, the magnitudes of terms I and IV are mostly far smaller than other terms so that they are hardly found to be visible in Fig. 10. Thus Fig. 12 is given to exhibit the term IV against term I, where the horizontal coordinate represents term I and the vertical coordinate represents term IV. It is clearly seen in Fig. 12**a** that the data points are mostly distributed in the fourth quadrant. This quantitative performance further underpins the inference from the above qualitative analysis, i.e., term I predominantly promotes PDI while term IV shows the completely reverse effect.

Term I in strategy 2 is the same as that in strategy 1. While an essential difference has to be noted in term IV is that its effect depends on the density change in the XLD−HYK−JHT reach. It is obvious that the attenuation of PDI due to term IV would be achieved, given the flow density decreases monotonically in the XLD−HYK−JHT reach. From Fig. 9, it is seen that the density decreases monotonically in most floods (Nos. 3~10,12,13,15~21). Consequently, one can readily deduce the reverse effects of term I in relation to term IV are evident in these floods, i.e., term I plays a facilitating role in PDI while term IV plays an inhibitory role (see Fig. 12**b**). Yet, also a few floods with non-monotonic changes of flow density are documented in Fig. 9. Specifically, the flow density decreases in the XLD−HYK reach but increases in the HYK−JHT reach for Nos.11,14 floods, which is in contrast to Nos.1,2 floods. It is hard to infer the effect of term IV for these floods with complex variation of the longitudinal density from a qualitative sense. By referring to the quantitative results, it is found that term IV promotes PDI in No.1 flood, and it attenuates PDI in Nos.2,11,14 floods. It is also noted that both term I and term IV play a role in promoting PDI in the No.2 flood. This indicates the effects of term I and term IV may not be rigorously opposite under the condition of a non-monotonic variation of flow density.

Furthermore, a significant feature deserves particular attention, that is, although term I is positive in most floods (e.g. Nos.2~21 flood), its magnitude is generally lower than term IV (see Fig. 12). From the quantitative results, considering the combined role of term I and term IV, an inhibiting effect on PDI due to the longitudinal density variation prevails in most floods (except Nos.1,2,8 flood in strategy 1, and

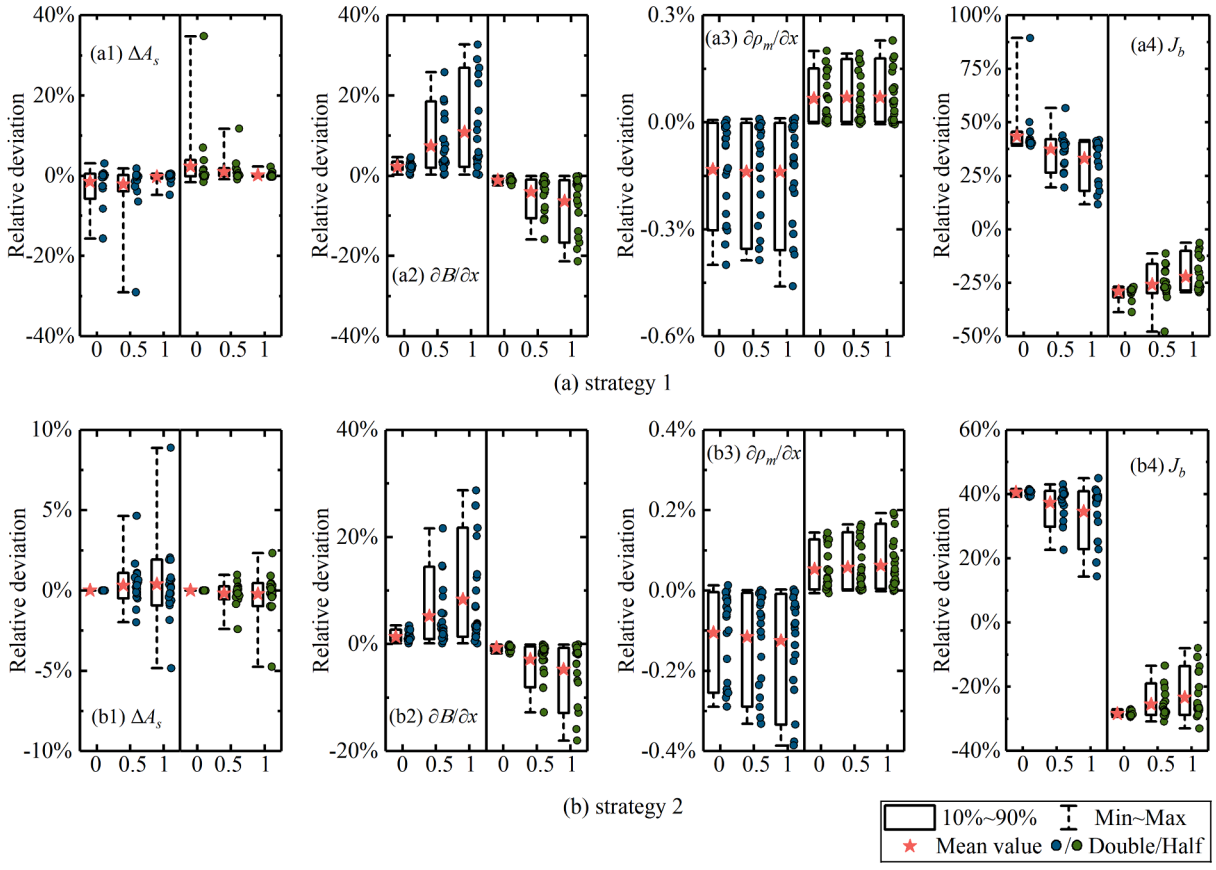

Fig. 15. Relative deviation range of roughness with the variation of ΔA_s, gradient of river width and flow density in (a) strategy 1 and (b) strategy 2. The horizontal coordinate represents three situations with weighting parameter of 0, 0.5, 1. The relative deviations of 21 floods are denoted by the scatter dots, and 10 % ~ 90 % of the data distributes in the box.

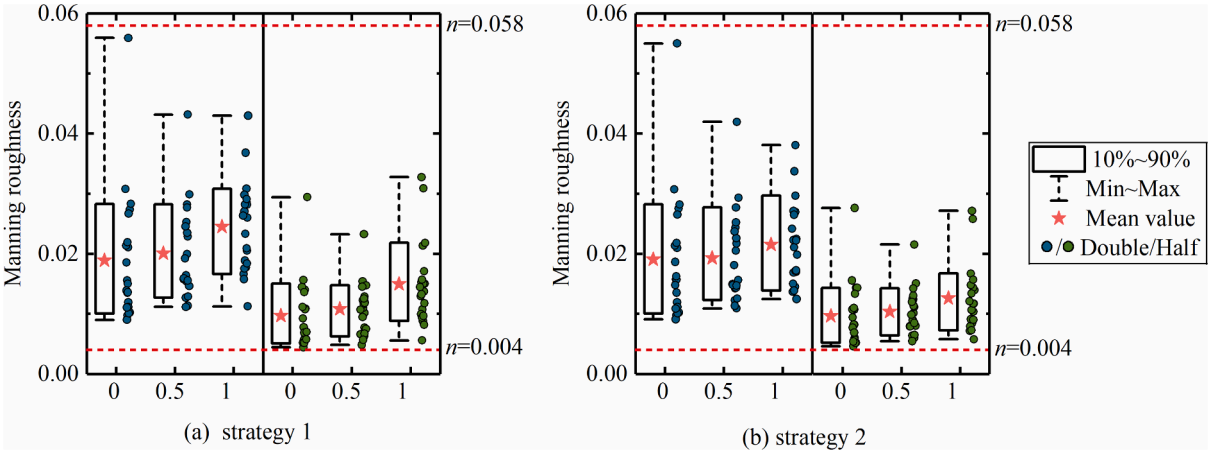

Fig. 16. The range of Manning roughness corresponds to the variation of bed slope in (a) strategy 1 and (b) strategy 2.

Nos.1,8,14 in strategy 2). Consequently, the longitudinal change of flow density mostly plays a role in inhibiting PDI, however, this effect is marginal with a sufficiently small magnitude.

3.2.2.3. Imbalanced advection transport. Term VII is an additional term due to the lower HYK−JHT reach is considered in strategy 2. It represents the effect of imbalanced advection transport, which is dependent on the difference of $\rho_m Q$ between XLD and JHT. According to the qualitative analysis, an increasing $\rho_m Q$ directed from XLD to JHT would promote PDI, and vice versa. The documented observation provides the respective features of the flow density and the flow discharge, which are the decomposition of $\rho_m Q$ (see Fig. 9). Specifically, the flow density and the flow discharge of XLD station are mostly greater than that of JHT station (except No.14 flood with a greater density and Nos.2,19,20 floods with a greater discharge at JHT station). Consequently, the product of the density and the discharge of XLD station is mostly greater than that of JHT station (except in No.19 flood). This results in a negative term VII to attenuate PDI for most floods. Also term VII has only a marginal influence on PDI, because its magnitude is comparatively small.

3.2.3. Uncertain factors

3.2.3.1. Longitudinal change of $\rho_m A$ due to the pressure gradient and advection. The effect of term II depends on the longitudinal variation of $\rho_m A$ (i.e., $\rho_m Bh$), It is recognized that a longitudinal decreasing $\rho_m Bh$ would promote PDI, and vice versa. Obviously the variations of the physical quantities, e.g., ρ_m, B, h may affect the value of the product $\rho_m Bh$. According to the field data (see Fig. 9), the river width increases in all floods, while the flow density (except Nos.1,2) and the water depth (except Nos.14,15,18,19) mostly decreases along the XLD−HYK reach. To clarify how the term II is affected by these physical quantities (ρ_m, B, h), further calculations of the spatial gradients of $\rho_m B$, Bh, and $\rho_m Bh$ are conducted. As shown in Fig. 13, the values of these gradients measure the longitudinal variations of $\rho_m B$, Bh, and $\rho_m Bh$, in which a positive value means increasing longitudinally and the reverse means decreasing longitudinally. Fig. 13**a** shows the gradients for the XLD−HYK reach corresponding to strategy 1. It is seen that $\rho_m B$, Bh, and $\rho_m Bh$ are longitudinally increases in most floods. The longitudinal increasing river width appears to be dominant in the variations of $\rho_m B$ and Bh due to the density and water depth are generally decrease. It is also noted that the longitudinal variation of $\rho_m Bh$ is basically in accordance with that of Bh (i.e., flow area). As a result, the negative term II always attenuate PDI (except No. 12).

In strategy 2, the effect of term II is dependent on the longitudinal variation of $\rho_m Bh$ between XLD and JHT. According to the field data (see Fig. 9), the river width increases (except Nos.8,15), while and the flow density (except No.14) and the water depth mostly decreases between XLD and JHT station. Fig. 13**b** shows the variations of $\rho_m B$, Bh, and $\rho_m Bh$ between XLD and JHT station. It is found that the $\rho_m B$ also increases in most floods, which is primarily ascribed to the increasing river width. However, it is hard to find out the predominant physical quantity that affects the longitudinal variation of Bh because of its uncertain performance, which increases in some floods (Nos.2,3,6,9,11,19~21) and decreases in other floods. Nevertheless, the longitudinal variation of $\rho_m Bh$ is also consistent with that of Bh in most of floods (except No.2). This means the effect of term II is indeed sophisticated, it plays a dual role in PDI, i.e., promoting or attenuating PDI in different floods.

3.2.3.2. Momentum term due to bed deformation. Term VI reflects the effect of momentum term caused by bed deformation, which is determined by not only the local bed deformation of the neighbouring stations, but also the value of weighting factor. Under the assumption of $\beta_1 = 1$ herein, term VI would promote PDI with the erosion of XLD in strategy 1. From Table 1, it is seen that the river bed is eroded (i.e., $\Delta A_s < 0$) at XLD station in more than a half of floods (Nos.1~9,16~19,21). Not surprisingly, the promoting effect of term VI in these floods (Nos.1~9,16~19,21) is expected according to the quantitative results.

In strategy 2, term VI is closely related to the longitudinal variation of ΔA_s. From Fig. 9, the ΔA_s varies monotonically only in a few floods (e.g., Nos.3,4,16,21 flood with a longitudinal increasing ΔA_s and Nos.15,18,19 flood with a longitudinal decreasing ΔA_s). Correspondingly, it is certain that term VI promotes PDI in Nos.3,4,16,21 flood, while it attenuates PDI in Nos.15,18,19 flood (see Fig. 11). There are some floods in which the ΔA_s varies non-monotonically (see Fig. 9). It is found that term VI promotes PDI in Nos.1,2,5~9,17 flood, in which the ΔA_s increases along the XLD−HYK reach and decreases along the HYK−JHT reach. In contrast, term VI attenuates PDI in Nos.10~14,20 flood, in which the ΔA_s decreases along the XLD−HYK reach and increases along the HYK−JHT reach. There is in fact reasonably good agreement between the quantitative performance of term VI and its qualitative analysis exclusively based on the XLD−HYK reach. This also suggests that the flow discharge increases at HYK station seem to be more sensitive to the bed deformation upstream of HYK station.

4. Discussion

4.1. Effects of the weighting parameters β_1 and β_2

From Eqs. (6-7), the weighting parameters β_1 and β_2 determines the relative contribution of two neighbouring stations (β_1 for M and F, β_2 for

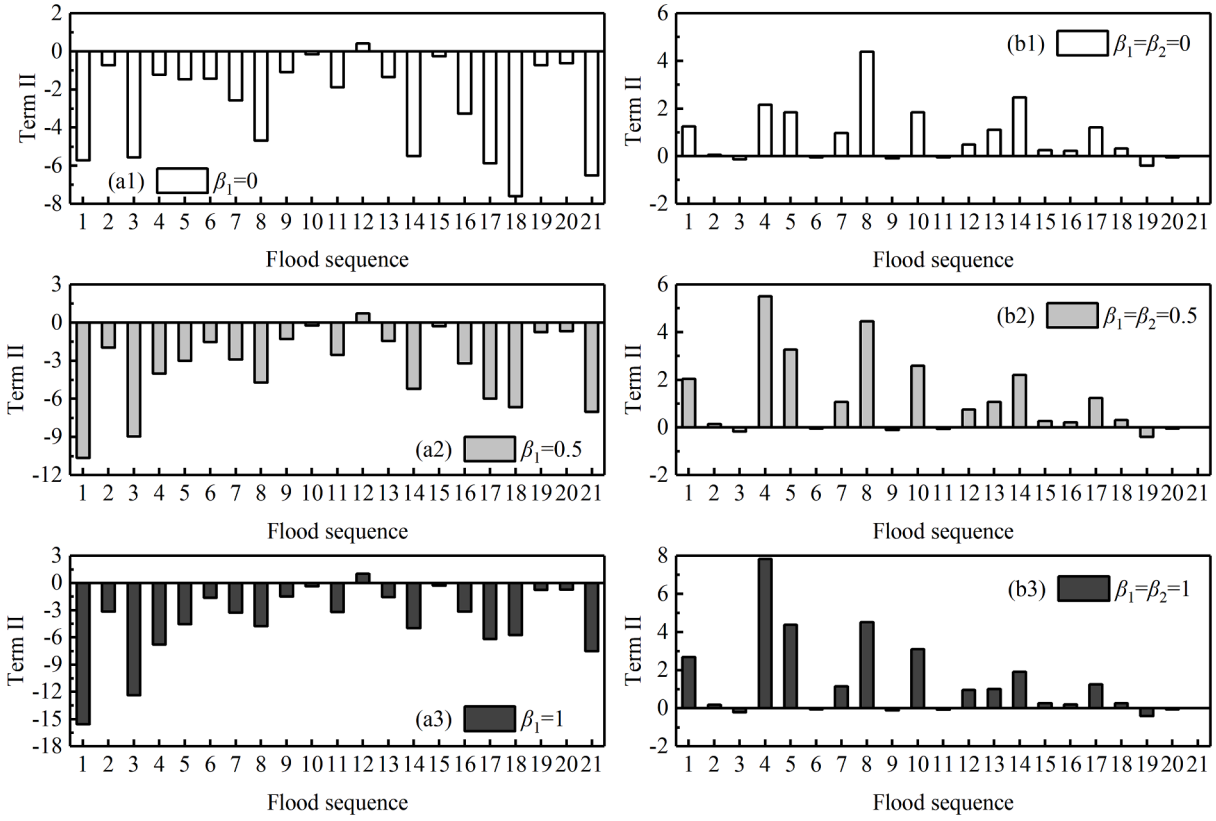

Fig. 17. Comparison of term II in (a1-a3) strategy 1 and (b1-b3) strategy 2.

N and F) on estimation of these seven factors. In section 3.2, results are obtained by setting $\beta_1 = \beta_2 = 1$. Here their effects are discussed by setting their values to 0 and 0.5. Fig. 14 presents the effects of weighting parameters on estimation of influencing terms. Firstly, it is seen that the responses of influencing terms to the increasing weighting parameter involve two tendencies, i.e., increasing either positively or negatively of the influencing terms in magnitude. A larger value of weighting parameter seems to mainly lead to a positive increasing trend for term III, relative to a negative increasing trend for term V and term VII. Yet uncertainties in changes of terms II, IV, VI remain as the weighting parameter increases. Secondly, variations of weighting parameters are inevitably affect the value of influencing terms in a quantitative sense, yet, the general impacts on PDI hold qualitatively for most terms, as presented above in Figs. 10-11. Nevertheless, it is noted that there are still a few terms, whose effects on PDI are rather sensitive to the change of weighting parameter. The most telling case is terms V and VI in strategy 1, the effects of which involve apparent inconsistency as the change of β_1 in some floods (e.g., Nos.3,5~9,15 for term V, and Nos.1~9,13~17,20 for term VI, the discrepancy of which are almost invisible in some floods because the small order of magnitude of terms, see Fig. 10). The discrepancy is justified because the deformation area as the key factor in term VI may show considerable discrepancy in neighbouring stations, which may indirectly affect term V. Irrespective of these minor variation, term III and term V always play the predominant role over all influencing terms regardless of the value of β_1 and β_2 for most floods. Finally, the considerable span of the circle points is seen relative to the diamond points, which concentrate near the origin. This indicates the difference as the change of weighting parameter appears to be enlarged for floods before 1999 relative to that after 1999, which may be ascribed to the difference features of PDI events after the completion of XLD reservoir. In summary, the weighting parameter has a marginal influence on the qualitative effects of terms. Though the values of influencing terms inevitably exhibit quantitative discrepancies with the change of weighting parameter, and may lead to the reverse effects for a few influencing terms that are sensitive to the weighting parameter. Nevertheless, their effects are substantiated comparatively weak on PDI in a quantitative sense. Therefore, the recognition that the effects of term III and term V prevail are invariable.

4.2. *Sensitivity of Manning roughness to estimated parameters*

4.2.1. *Performance of sensitivity metric*

In this study, the accuracy of the estimated discharge variation depends on the precise knowledge of parameters involved in the Eqs. (8-9). However, it is difficult to determine the parameters with highly complex evolution during the spatial and temporal development of the fluvial process, due to the fact that synchronous accurate field measurements are lacking. This necessitates simplified estimations for some parameters in poorly available data occasions. For example, multiple distinct peak discharges may successively ensue over the whole ongoing flood season, severely limiting the conduct of field surveys for individual floods. This leads to the real-time measurements of bed deformation during the flood season are prohibitively difficult to make. Therefore, the bed deformation data for the multiple floods in the same year used in this study are identical. Similarly, parameters like the gradient of river width, the gradient of flow density, and bed slope are also uncertain with longitudinal heterogeneity due to the absence of measurements between the adjacent stations. Herein, the assumption of linear variation approximately for these parameters is employed to address this point. To gain further insights into the potential error due to these approximation constraints on the parameters, we recalculate the Manning roughness after multiplying these parameters by factors of 2 and 0.5, respectively. The relative deviation of roughness value (i.e., the relative deviation $R_n = (n_* - n)/n$, where n_* represents the value of Manning roughness calculated by doubled parameter or halved parameter, and n is the back-estimated roughness value in Section 3.1) makes it available for

assessing the sensitivity of the approximation.

Fig. 15 shows the relative deviations of roughness for the variation of ΔA_s, $\frac{\partial B}{\partial x}$, $\frac{\partial \rho_m}{\partial x}$, and J_b. In Fig. 15, the horizontal coordinate denotes different values of weighting parameter, the relative deviations of 21 floods are denoted by the scatter dots, and the box represents the distribution range of 10 % ~ 90 % of the data. From Fig. 15, the maximum average deviations corresponding to the variations (including doubled and halved) of ΔA_s, $\frac{\partial B}{\partial x}$, $\frac{\partial \rho_m}{\partial x}$, and J_b are 2.3 %, 10.8 %, −0.14 %, and 43.5 % in strategy 1, while that in strategy 2 are 0.4 %, 8.3 %, −0.12 %, and 40.6 %, respectively. It is apparent that the slight deviations for the parameters ΔA_s, $\frac{\partial B}{\partial x}$, $\frac{\partial \rho_m}{\partial x}$ are generally satisfactory. Yet, the deviation of the roughness value in line with the variation of J_b appears to be unexpected. With the variation of bed slope, a comparatively large error tolerance is attained, which even amounts to 89 % and 45 % in strategy 1 and strategy 2, respectively. In this regard, Fig. 16 is papered to exhibit the values of Manning roughness for the variation of bed slope. It is seen in Fig. 16 that the values of roughness are entirely within a rational range determined by the rare measured data, indicating the applicability of the roughness even with varied bed slopes. In general, although the Manning roughness is rather sensitive to the variation of bed slope, the simplified assumption has only a marginal influence on the estimation.

4.2.2. Restriction of sensitivity verification

A pivotal issue about the approach to testing sensitivity merits attention. Indeed, flood propagation is accompanied by energy conversion from upstream to downstream. During the process, intimate relationships are not only developed between the hydraulic parameters but also between the upstream and downstream stations. Yet, the treatment of exclusively changing the tested parameter to recalculate roughness value may bring uncertainty to the application in actual floods. In present study, such a particular case occurs in the No.8 flood with $\beta_1 = 0$ of strategy 1. It is apparent that the value of Manning roughness can be obtained by $T = \rho_m g A J_f = \rho_m g A \frac{n^2 (Q/A)^2}{h^{4/3}}$, one has to pre-determine the value of T during the back-estimation to solve for roughness. However, a negative resistance T is obtained by $T = \rho_m g h^2 \frac{\partial B}{\partial x} + gA(h - h_c)\frac{\partial \rho_m}{\partial x} + G' - C$ during the back-estimation, resulting in no solution for roughness under this circumstance. This is because the parameter C is sufficiently large to lead to a negative T on the premise of other items are positive in this expression. Thereby, a large value of E is required to figure out the sufficiently large value of C. Following Eq. (7a), E_1 can be calculated by $E_1 = \frac{[(\rho_m Q)_E - (\rho_m Q)_M] + D_1[(\rho_m A)_E - (\rho_m A)_M] - K_1}{\Delta t}$, from which a larger value of E_1 can be obtained by the negative K_1 or a smaller Δt. Accordingly, the No.8 flood is featured by heavy deposition of riverbed and the short propagation time of flood peak. The former leads to a large E_1 by affecting K_1, and the latter provides a small Δt, both of which contribute to a negative T.

4.3. Evaluation of strategies

Present two strategies in this study have led to the recognition that the most predominant factors spurring PDI events are the pressure term due to the river width gradient (term III) and the external force term (term V). Yet, quantitative differences in influencing terms are expected due to distinct approaches to applying the ODEs for evaluating the discharge variation. Following the Eqs. (8-9) deduced by these approaches, the differences in each term arise from the different river reach adopted to solve discharge at HYK. The XLD−HYK reach upstream of the HYK is used in strategy 1, while the upstream (XLD−HYK) and downstream (HYK−JHT) reach of the HYK both are used in strategy 2. In strategy 2, term VII is added to represent the influence of discharge change between upstream and downstream. Nevertheless, term VII has a marginal effect on PDI in terms of its magnitude. Instead, a more marked distinction occurs in term II. To better compare its influence, the value of term II is divided by the discharge increment, as shown in Fig. 17. Term II mostly inhibits PDI in strategy 1 but promotes PDI in strategy 2. This is because the longitudinal variation of $\rho_m A$ increases in XLD−HYK reach of strategy 1, but rather, decreases in XLD−JHT reach of strategy 2 (see Fig. 13 (a3, b3)).

Of more interest is which strategy can explain the causes of PDI precisely. It requires a reliable analysis based on the field data during floods for validation not only from a qualitative perspective but also from a quantitative perspective. Some previous studies have provided valuable insights into the primary causes of PDI from a qualitative sense, however, these studies mostly focus on the predominant causes in a few specific floods. It is appreciated that whether the flood peak increases or decreases is a very complicated process that depends on the interaction of multiple factors according to the analysis in this study. Yet the causes with a marginal influence on PDI have rarely been incorporated in the aforementioned studies. In addition, the quantitative analysis based upon field data is mostly hindered by the insufficient consecutive observations. As such, the applicability in practice of the two strategies remains to be verified. However, a basic consensus that should be reached is that the primary influencing factors of PDI (i.e., term III and term V) are identical in both strategies.

5. Conclusions

The ordinary differential equations along the characteristics are derived from the cross sectional-integrated continuity and momentum equations for sediment-laden flows. Two strategies are proposed to use the derived equations for evaluating the discharge variation, from which seven factors that may affect the PDI are obtained. The seven influencing factors of PDI are further quantified by applying the hydrological data of 21 floods during 1973–2012 in the Lower Yellow River to reveal new insights into the mechanisms for PDI. The following conclusions are drawn from this study:

The PDI phenomenon caused by the hyperconcentrated floods appears more intense after the completion of XLD Reservoir with 2.4 times increment and 1.5 times frequency higher than before.

The PDI is a complicated process depending on the interaction of multiple factors, involving the effects of the flow density change on the upstream discharge (term I), the longitudinal change of $\rho_m A$ due to the pressure gradient and advection (term II), the pressure term due to the river width gradient (term III), the pressure term due to the flow density (term IV), the external forces composed of gravity and resistance (term V), the momentum term due to bed deformation (term VI), and the imbalanced advection (term VII).

The quantitative comparison of influencing factors confirms that the effects of term III and term V prevail, whereas other influencing terms are minor. Specifically, the PDI is mostly promoted by the positive pressure term III due to the longitudinal increasing river width, while it is attenuated by the external forces (term V), the imbalanced advection transport (term VII), and the combined role of terms I and IV related to the longitudinal decreasing density. Yet, the effects of term II and term VI remain uncertain because the appreciable discrepancy of the performance in different floods.

Uncertainty is inevitable due to the uniqueness of each flood and the approximation constraints for insufficient observations. Nevertheless, the consensus of PDI can be reached in this study on the basis of the commonalities of most floods by reasonable assumption and approximation. This is sensible, given the fact that precise estimation of each flood is hard to carry out at present due to the lacking of available data. Additionally, the quantification in the present study tentatively provides an approach to realizing the mechanism of PDI in a physical sense, which facilitates the enhanced understanding of the reasons for PDI.

CRediT authorship contribution statement

Wei Li: Conceptualization, Methodology, Investigation, Writing – original draft, Writing – review & editing, Supervision. **Lehong Zhu:**

Formal analysis, Writing – original draft, Writing – review & editing, Visualization. **Guohu Xie:** Formal analysis, Visualization. **Peng Hu:** Conceptualization, Methodology, Writing – review & editing, Supervision. **Huib J. de Vriend:** Writing – review & editing.

Declaration of Competing Interest

The authors declare that they have no known competing financial interests or personal relationships that could have appeared to influence the work reported in this paper.

Data availability

The data that has been used is confidential.

Acknowledgements

This work is supported by the National Natural Science Foundation of China (No. 11872332, 12172331), and the Key Laboratory Project of Yellow River Sediments under Chinese Ministry of Water Resources (No. K18-529112-013).

References

Cao, Z.X., Pender, G., Carling, P., 2006. Shallow water hydrodynamic models for hyperconcentrated sediment-laden floods over erodible bed. Adv. Water Resour. 29, 546–557. https://doi.org/10.1016/j.advwatres.2005.06.011.

Cao, Z.X., Li, Z.J., Pender, G., Hu, P., 2012. Non-capacity or capacity model for fluvial sediment transport. Proc. Inst. Civ. Eng.: Water Manag. 165, 193–211. https://doi.org/10.1680/wama.10.00035.

Chien, N., 1989. A Study of Hyperconcentrated Flows. Tsinghua University Press, Beijing in Chinese.

Chien, N., Wan, Z.H., 1999. Mechanics of sediment transport. ASCE Press. https://doi.org/10.1061/9780784404003.

Ding, Y., Zhong, D.Y., Zhang, H.W., 2010. Study on the mechanism of flood peak discharge increasing in sediment-laden rivers based on characteristic analysis. J. Hydroelectr. Eng. 29, 202–208 in Chinese.

Dong, W.S., Jiang, X.F., He, X.F., Zai, Y.Y., 2012. Study on the clay mechanical characteristics of "ripping up the bottom" in the Yellow River. Appl. Mech. Mater. 212–213, 108–112. https://doi.org/10.4028/www.scientific.net/AMM.212-213.108.

Dou, S.T., Zhang, Y.F., Yu, X., Yang, M., 2014. Dynamics mechanism analysis and process of sediment-hyperconcentrated flood routing. J. Hydroelectr. Eng. 33, 114–119 in Chinese.

Einstein, H.A., Chien, N., 1955. Effects of heavy sediment concentration near the bed on velocity and sediment distribution. MRD Sediment Seeries 8. University of California, Berkeley.

Engelund, F., Wan, Z.H., 1984. Instability of hyperconcentrated flow. J. Hydraul. Eng. 110, 219–233. https://doi.org/10.1061/(ASCE)0733-9429(1984)110:3(219).

Gust, G., 1976. Observations on turbulent-drag reduction in a dilute suspension of clay in sea-water. J. Fluid Mech. 75, 29–47. https://doi.org/10.1017/S0022112076000116.

Jiang, E.H., Zhao, L.J., Wei, Z.L., 2006. Mechanism of flood peak increase along the Lower Yellow River and its verification. J. Hydraul. Eng. 37, 1454–1459. https://doi.org/10.13243/j.cnki.slxb.2006.12.008 in Chinese.

Kuang, S.F., Xu, Y.N., Wang, L., Li, W.W., 1999. Mechanism of ripping up the bottom due to hyperconcentrated flow. In: Jayawardena, A.W., Lee, J.H., Wang, Z.Y. (Eds.), River Sedimentation: Theory and Applications. A.A. Balkema, Rotterdam, pp. 283–288.

Li, G.Y., 2008. Analysis on mechanism of peak discharge increasing during flood routing in lower reaches of Yellow River. J. Hydraul. Eng. 39, 511–517. https://doi.org/10.13243/j.cnki.slxb.2008.05.007 in Chinese.

Li, W., Van Maren, D.S., Wang, Z.B., de Vriend, H.J., Wu, B.S., 2014. Peak discharge increase in hyperconcentrated floods. Adv. Water Resour. 67, 65–77. https://doi.org/10.1016/j.advwatres.2014.02.007.

Li, W., Su, Z.H., van Maren, D.S., Wang, Z.B., de Vriend, H.J., 2017. Mechanisms of hyperconcentrated flood propagation in a dynamic channel-floodplain system. Adv. Water Resour. 107, 470–489. https://doi.org/10.1016/j.advwatres.2017.05.012.

Ma, H.B., Nittrouer, J.A., Naito, K., Fu, X.D., Zhang, Y.F., Moodie, A.J., Wang, Y., Wu, B., Parker, G., 2017. The exceptional sediment load of fine-grained dispersal systems: Example of the Yellow River, China. Sci. Adv. 3, e1603114.

Ma, H.B., Nittrouer, J.A., Fu, X.D., Parker, G., Zhang, Y.F., Wang, Y.J., Wang, Y.J., Lamb, M.P., Cisneros, J., Best, J., Parsons, D.R., Wu, B.S., 2022. Amplification of downstream flood stage due to damming of fine-grained rivers. Nat. Commun. 13, 3054. https://doi.org/10.1038/s41467-022-30730-9.

Qi, P., Li, W.X., 1996. Evolutional characteristics of hyper-concentrated flow in braided channel of the Yellow River. Int. J. Sediment. Res. 11, 49–57.

Qi, P., Sun, Z.Y., Qi, H.H., 2011. Research on two-bank training strategy for wandering channels of Lower Yellow River. J. Sediment. Res. 1–9 https://doi.org/10.16239/j.cnki.0468-155x.2011.03.003 in Chinese.

Qi, P., Sun, Z.Y., 2013. Discussion on reasons for peak discharge increasing during flood routing in lower reaches of Yellow River. in Chinese J. Hydraul. Eng. 44, 1002–1007. https://doi.org/10.13243/j.cnki.slxb.2013.08.005.

Singh, D.K., Xu, M.Z., Singh, N., Lei, F.K., 2021. Perspectives on emerging pressures and their integrated impact on large river systems: An insight from the Yellow River basin. J. Environ. Manag. 298, 113423 https://doi.org/10.1016/j.jenvman.2021.113423.

Tian, S.M., Xu, M.Z., Jiang, E.H., Wang, G.H., Hu, H.C., Liu, X., 2019. Temporal variations of runoff and sediment load in the upper Yellow River, China. J. Hydrol. 568, 46–56. https://doi.org/10.1016/j.jhydrol.2018.10.033.

Van Maren, D.S., Winterwerp, J.C., Wang, Z.Y., Qi, P., 2009a. Suspended sediment dynamics and morphodynamics in the Yellow River, China. Sedimentol. 56, 785–806. https://doi.org/10.1111/j.1365-3091.2008.00997.x.

Van Maren, D.S., Winterwerp, J.C., Wu, B.S., Zhou, J.J., 2009b. Modelling hyperconcentrated flow in the Yellow River. Earth Surf. Process. Landforms 34, 596–612. https://doi.org/10.1002/esp.1760.

Vanoni, V.A., 1946. Transportation of suspended sediment by water. Trans. Am. Soc. Civ. Eng. 111, 67–102. https://doi.org/10.1061/TACEAT.0005975.

Wan, Z.H., 1985. Bed material movement in hyperconcentrated flow. J. Hydraul. Eng. 111, 987–1002. https://doi.org/10.1061/(ASCE)0733-9429(1985)111:6(987).

Wan, Z.H., Wang, Z.Y., 1994. Hyperconcentrated Flow, first ed. CRC Press, London.

Wang, Z.Y., 2002. Free surface instability of non-Newtonian laminar flows. J. Hydraul. Res. 40, 449–460. https://doi.org/10.1080/00221680209499887.

Wang, Z.Y., Chien, N., 1984. Experimental study on the physical properties of sediment suspensions with hyperconcentration. J. Hydraul. Eng. 1–10 https://doi.org/10.13243/j.cnki.slxb.1984.04.001 in Chinese.

Wang, Z.Y., Liu, C., 2019. Two-thousand years of debates and practices of Yellow River training strategies. Int. J. Sediment. Res. 34, 73–83. https://doi.org/10.1016/j.ijsrc.2018.08.006.

Wang, Z.Y., Larsen, P., Nestmann, F., Dittrich, A., 1998. Resistance and drag reduction of flows of clay suspensions. J. Hydraul. Eng. 124, 41–49. https://doi.org/10.1061/(ASCE)0733-9429(1998)124:1(41).

Wang, Z.Y., Qi, P., Melching, C.S., 2009. Fluvial hydraulics of hyperconcentrated floods in Chinese rivers. Earth Surf. Process. Landforms 34, 981–993. https://doi.org/10.1002/esp.1789.

Wang, Z.J., Xu, M.Z., Liu, X., Singh, D.K., Fu, X.D., 2022. Quantifying the impact of climate change and anthropogenic activities on runoff and sediment load reduction in a typical Loess Plateau watershed. J. Hydrol. Reg. Stud. 39, 100992 https://doi.org/10.1016/j.ejrh.2022.100992.

Winterwerp, J.C., 2001. Stratification effects by cohesive and noncohesive sediment. J. Geophys. Res. Oceans 106, 22559–22574. https://doi.org/10.1029/2000JC000435.

Winterwerp, J.C., 2006. Stratification effects by fine suspended sediment at low, medium, and very high concentrations. J. Geophys. Res. 111, C05012. https://doi.org/10.1029/2005JC003019.

Winterwerp, J.C., Lely, M., He, Q., 2009. Sediment-induced buoyancy destruction and drag reduction in estuaries. Ocean. Dyn. 59, 781–791. https://doi.org/10.1007/s10236-009-0237-y.

Wu, W.M., Wang, S.S.Y., 2007. One-dimensional modeling of dam-break flow over movable beds. J. Hydraul. Eng. 133, 48–58. https://doi.org/10.1061/(ASCE)0733-9429(2007)133:1(48).

Wu, B.S., Xia, J.Q., Fu, X.D., Zhang, Y.F., Wang, G.Q., 2008. Effect of altered flow regime on bankfull area of the Lower Yellow River, China. Earth Surf. Process. Landforms 33, 1585–1601. https://doi.org/10.1002/esp.1679.

Xu, M.Z., Wang, G.H., Wang, Z.J., Hu, H.C., Singh, D.K., Tian, S.M., 2022. Temporal and spatial hydrological variations of the Yellow River in the past 60 years. J. Hydrol. 609, 127750 https://doi.org/10.1016/j.jhydrol.2022.127750.

Zhang, R.J., 1963. A review of the gravitation theory of sediment suspension. J. Hydraul. Eng. 11–23 https://doi.org/10.13243/j.cnki.slxb.1963.03.002 in Chinese.

Zhong, D.Y., Yao, Z.Y., Zhang, L., Liu, L., 2013. Amplification of non-inundating hyperconcentrated flood waves and criterion of its occurred. in Chinese J. Hydraul. Eng. 44, 50–58. https://doi.org/10.13243/j.cnki.slxb.2013.01.012.

Zhu, C.J., Hao, Z.C., 2008. A study on the resistance reduction of flows with hyper-concentration in open channel, in: 2008 International Workshop on Education Technology and Training & 2008 International Workshop on Geoscience and Remote Sensing. Presented at the 2008 International Workshop on Geoscience and Remote Sensing (ETT and GRS), IEEE, Shanghai, China, pp. 141–144. doi:10.1109/ETTandGRS.2008.172.